Physics Reports 521 (2012) 69–94

Contents lists available at SciVerse ScienceDirect

Physics Reports

journal homepage: www.elsevier.com/locate/physrep

Single photon frequency up-conversion and its applications☆

Lijun Ma, Oliver Slattery, Xiao Tang *

Information Technology Laboratory, National Institute of Standards and Technology, 100 Bureau Dr., Gaithersburg, MD 20899, United States

ARTICLE INFO

Article history:
Accepted 31 July 2012
Available online 21 August 2012
editor: J. Eichler

Keywords:
Frequency up-conversion
Single photon detection
Quantum information

ABSTRACT

Optical frequency up-conversion is a technique, based on sum frequency generation in a non-linear optical medium, in which signal light from one frequency (wavelength) is converted to another frequency. By using this technique, near infrared light can be converted to light in the visible or near visible range and therefore detected by commercially available visible detectors with high efficiency and low noise. The National Institute of Standards and Technology (NIST) has adapted the frequency up-conversion technique to develop highly efficient and sensitive single photon detectors and a spectrometer for use at telecommunication wavelengths. The NIST team used these single photon up-conversion detectors and spectrometer in a variety of pioneering research projects including the implementation of a quantum key distribution system; the demonstration of a detector with a temporal resolution beyond the jitter limitation of commercial single photon detectors; the characterization of an entangled photon pair source, including a direct spectrum measurement for photons generated in spontaneous parametric down-conversion; the characterization of single photons from quantum dots including the measurement of carrier lifetime with escalated high accuracy and the demonstration of the converted quantum dot photons preserving their non-classical features; the observation of 2nd, 3rd and 4th order temporal correlations of near infrared single photons from coherent and pseudo-thermal sources following frequency up-conversion; a study on the time-resolving measurement capability of the detectors using a short pulse pump and; evaluating the modulation of a single photon wave packet for better interfacing of independent sources. In this article, we will present an overview of the frequency up-conversion technique, introduce its applications in quantum information systems and discuss its unique features and prospects for the future.

Published by Elsevier B.V.

Contents

☆ The identification of any commercial product or trade name does not imply endorsement or recommendation by the National Institute of Standards and Technology.

* Corresponding author.
E-mail address: xiao.tang@nist.gov (X. Tang).

0370-1573/$ – see front matter. Published by Elsevier B.V.
doi:10.1016/j.physrep.2012.07.006

1. Introduction

The performance of a quantum information system depends on both transmission loss and detection efficiency. For fiber-based quantum information systems, the near infrared (NIR) telecommunication wavelength bands (1310 and 1550 nm) have the lowest transmission loss. The performance of single photon detectors for telecommunication wavelength bands is therefore a key issue for quantum communication systems. Refs. [1,2] list a variety of single photon detectors and compare their performances. Based on [1,2], we list the most commonly used single photon detectors in Table 1.

Currently, the most efficient and low cost single photon detector technology is the silicon based avalanche photodiode (Si-APD) which has a very high detection efficiency and very low dark-count rate in the visible wavelength range (see Table 1). Unfortunately, it does not operate in the NIR wavelength bands. Commercially available indium–gallium–arsenic (InGaAs) based APDs can be operated as single-photon detectors in the NIR wavelength bands, however they suffer from low detection efficiency, high noise and severe after-pulsing that reduces the maximum possible count rate significantly. Therefore, InGaAs APDs are typically operated in a gated mode, limiting their application in high-speed quantum information systems. To overcome this application limit, InGaAs APDs with self-differencing techniques were developed to meet the requirements for high speed quantum communication systems [3]. Despite this, however, InGaAs detectors are difficult to operate in free-running mode and not suitable for applications with very low signal photon flux due to their relatively high dark-count rate. A variety of superconducting single-photon detectors (SSPDs) have been developed in the research community [1,2]. They can be categorized into two commonly used types: transition edge sensor (TES) [4] and superconducting nanowire single photon detector (SNSPD) [5–7]. The TES can reach almost 100% detection efficiency with photon number resolving capability but displays a long timing jitter (100 ns). In contrast, the SNSPD has much shorter timing jitter (30–60 ps) but its detection efficiency is low (1% or 2%). A specially designed SNSPD with an integrated optical cavity and suitable anti-reflection coating was reported in 2006 [8] showing a detection efficiency of 57% at 1550 nm. These two types of superconducting single photon detectors show superior performance and are suitable for a variety of applications in the NIR wavelength bands. However, they require cryogenic operating temperatures which significantly increases cost and complexity, and are currently not widely commercially-available.

In order to use Si-APDs for the detection of single photons in the NIR telecommunication wavelengths, we use a non-linear optical medium to convert the wavelength of photons in the NIR range to a shorter wavelength in the visible or near visible range. This is a frequency up-conversion process, typically referred to as sum frequency generation (SFG), since the low frequencies are up-converted to higher frequencies. The emerging photons at the visible wavelengths are then suitable for efficient detection using a Si-APD. This type of single photon detector is usually called an up-conversion detector.

The first experiment for optical frequency up-conversion was performed in 1967 [9]. Frequency conversion at the single photon level has been studied since 1990 [10], when Kumar predicted that the quantum state of single photons can be preserved during the frequency conversion process. In 1992, Huang and Kumar experimentally showed that the non-classical intensity correlation between twin beams at 1064 nm was preserved after one beam was frequency up-converted to a wavelength of 532 nm [11]. In 2001, Kim and colleagues used up-conversion to implement a complete Bell state measurement in a quantum teleportation scheme [12]. Since 2004, several groups have successfully developed highly efficient frequency conversion at single photon levels by using periodically poled lithium niobate (PPLN) bulk or waveguide devices [13–18].

We adapted this technology and developed high efficiency and low noise up-conversion detectors for single photon detection near 1310 nm [18]. The total detection efficiency of our up-conversion detectors is 32% with a dark-count rate of 2200/s at the peak detection efficiency. Our recent experiment shows that the dark-count rate can be further reduced to 650/s when a strict filtration scheme is used. The timing jitter in the up-conversion detectors is generated in the Si-APD used, which is about 400 ps. The maximum count rate of 10 MHz is also limited by the Si-APD. Up-conversion detectors can be operated in a free-running mode as well as a pulsed (optically gated) mode. Up-conversion detectors can be built entirely using commercially available components and routinely operated at room or a moderately elevated localized temperature. Based on the up-conversion detector, we have also implemented a highly sensitive single photon up-conversion spectrometer [19] by using a tunable laser as the pump source.

To demonstrate the range of applications for these devices, we used the up-conversion detectors developed at NIST for the following:

1. A high speed fiber-based quantum key distribution (QKD) system at 1310 nm [20];
2. Multiple wavelength optical pumping of a detector which enables a higher temporal resolution beyond the Si-APD timing jitter limitation in communication systems [21];

Table 1
Comparison of most commonly used single photon detectors.

Detector type	Operation temp. (K)	Detection efficiency, wavelength η (%), λ (nm)	Timing jitter δt (ns) (FWHM)	Dark-count rate, D (ungated) (1/s)	Max. count rate (10^6/s)
PMT (infrared)	200	2@1550	0.3	200 000	10
Si-APD (thick)	250	65@650	0.4	25	10
Si-APD (shallow)	250	49@550	0.035	25	10
InGaAs APD (gated)	200	10@1550	0.37	91(gated)	0.01
InGaAs APD (self-diff.)	240	10@1550	0.055	16 000	100
TES(W)	0.1	95@1556	100	…	0.1
SNSPD	3	0.7@1550	0.06	10	100
SNSPD (in cavity)	1.5	57@1550	0.03	…	1000

3. Characterization of entangled photon sources, including single photon level spectrum measurements and two photon interferences [22];
4. Characterization of photons from semiconductor quantum dots, including measurements of spectrum, lifetime and second order correlation for the photons [23];
5. High-orders of photon correlation following frequency conversion [24];
6. Amplitude modulation of single photons during frequency conversion [25].

These applications demonstrate that single photon frequency up-conversion is a versatile technique in quantum information research.

2. Single photon frequency up-conversion

2.1. Frequency up-conversion

Frequency up-conversion is a non-linear optical phenomenon, in which two input photons (a signal and a pump photon) at different frequencies annihilate and another photon at their sum frequency is simultaneously generated in the non-linear optical medium. To achieve high conversion efficiency, we insert a strong pump laser at angular frequency ω_p and a very weak optical signal at ω_s into a nonlinear material to generate an output signal at ω_o. According to non-linear optics theory [26,27], this annihilation of the pump and signal photons to produce a new output photon can happen only if both the energy and momentum involved in the process are preserved. Eq. (1a) is derived from the conservation of energy and Eq. (1b) is derived from the conservation of momentum.

$$\omega_s + \omega_p = \omega_o \tag{1a}$$

$$\vec{k}_s + \vec{k}_p = \vec{k}_o \tag{1b}$$

where $\vec{k}_s$, $\vec{k}_p$ and $\vec{k}_o$ are the wave vectors of the signal, pump and the output light. From Eqs. (1a) and (1b), we can write the phase matching conditions as:

$$n_s\omega_s + n_p\omega_p = n_o\omega_o \tag{2}$$

where n_s, n_p and n_o are the refractive indexes of the material at the signal, pump and output frequencies, respectively. The most commonly used optical media for frequency conversion are non-linear crystals, which are dispersive materials, (i.e. the refractive index is wavelength dependent). It is impossible to satisfy Eq. (2) if the three light beams have the same polarization. In practice, we can use the birefringence of the crystal to satisfy the phase matching condition by careful selection of incident angle and polarization direction of the input beams with respect to the orientation of the birefringent crystal. The advantage of birefringence phase matching is that it is perfect phase matching. However, the following limitations apply:

1. Wavelength selection is limited by the birefringent refractive index of the crystal and the orientations of the respective beams. In another words, we cannot always find a suitable crystal material and beam orientation angle for all wavelengths to achieve phase matching.
2. Along the crystal orientation with the highest nonlinear coefficient, it is usually not possible for birefringent phase-matching. In another words, usable nonlinear coefficients are relatively low.
3. Birefringent phase-matching suffers from walk-off, in which the extraordinary part (e-ray) and the ordinary part (o-ray) of the beam in the crystal travel in different directions. This walk-off limits the interaction length and thus reduces the internal conversion efficiency.

Due to these limitations, birefringent phase matching cannot be used to implement highly efficient frequency conversion, and is therefore not suitable for up-conversion detectors. An alternative approach called quasi-phase matching (QPM) was developed that allows collinear pump and signal beams of the same polarization to be used in a periodically poled bulk or waveguide nonlinear medium. In QPM, the crystal axis is periodically flipped. In each poling domain width, there is a

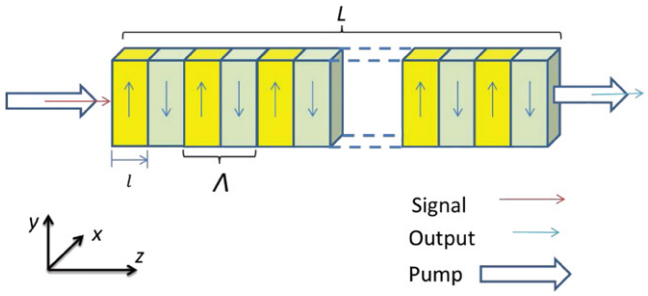

Fig. 1. Schematic diagram of a PPLN bulk device for sum frequency generation.

small amount of phase mismatch which is reversed, or canceled, during the next oppositely flipped poling domain, thereby ensuring that there is a continuous positive energy conversion from the signal and pump beams to the output beam despite all three beams being collinear and having the same polarization. Having all beams collinear overcomes the problem of walk-off. Additionally, since all beams are aligned to the same extraordinary polarization mode, we can take advantage of the highest non-linear coefficients in the crystal.

The basic theory of the birefringent phase-matched evolution of three waves can be adapted into QPM interaction in a periodically poled bulk medium with the substitution that the nonlinear coefficient of the medium is periodically modulated (Fig. 1).

The relations that describe the nonlinear field evolution in a periodically poled nonlinear medium were given by Myers et al. [28]. In this case, the nonlinear coefficient is substituted by a Fourier series representation of periodically modulated nonlinear coefficient:

$$d(z) = d_{eff} \sum_{m=-\infty}^{\infty} G_m \exp(-ik_m z) \tag{3}$$

where d_{eff} is the effective nonlinear coefficient of the same process in a uniform bulk material, $k_m = 2\pi m/\Lambda$ is the grating vector of the mth Fourier component, Λ is the period of the modulated structure, and G_m is the Fourier coefficient. If we ignore the non-phase-matched components and only take the phase-matched components into account, the coupled equations describing the interacting waves become:

$$\frac{dE_s}{dz} = i\frac{\omega_s d_Q}{n_s c} E_p E_o \cdot \exp(-i\Delta k_Q z), \tag{4a}$$

$$\frac{dE_o}{dz} = i\frac{\omega_o d_Q}{n_o c} E_p E_s \cdot \exp(-i\Delta k_Q z), \tag{4b}$$

$$\frac{dE_p}{dz} = i\frac{\omega_p d_Q}{n_p c} E_s E_o \cdot \exp(-i\Delta k_Q z). \tag{4c}$$

where E_j, ω_j and n_j are the electrical field, angular frequency and refractive index with the subscript $j = s$ for signal, $j = o$ for sum frequency output and $j = p$ for pump, c is the vacuum speed of light. From the Fourier expansion, the effective nonlinear coefficient for the QPM interaction is:

$$d_Q = d_{eff} G_m \tag{5}$$

The wave-vector mismatch for the QPM interaction is:

$$\Delta k_Q = k_o - k_s - k_p - k_m \tag{6}$$

where k_p, k_s, k_o are the wave vectors of the pump, the signal and the SFG output, respectively, in the case that all wave vectors are collinear with the grating vector. In a PPLN structure, the nonlinear coefficient periodically changes its sign, and the Fourier coefficient is:

$$G_m = \frac{2}{m\pi} \sin(m\pi D) \tag{7}$$

where the duty factor, $D = l/\Lambda$, is given by the length, l, of a reversed domain divided by the period, Λ, of the reversal. For the first-order QPM process ($m = 1$) at the boundary between two adjacent and oppositely poled domains (50% duty factor), the effective nonlinear coefficient is the largest: $d_Q = (\frac{2}{\pi}) d_{eff}$. The wave-vector mismatch for the first-order QPM collinear process is:

$$\Delta k_Q = k_o - k_s - k_p - \frac{2\pi}{\Lambda}. \tag{8}$$

The poling period, Λ, is then determined by the QPM condition:

$$\Lambda = \frac{2\pi}{k_o - k_s - k_p}. \tag{9}$$

The theory of three-wave mixing in waveguides is mathematically equivalent to a plane-wave interaction and permits complete energy conversion from one wavelength to another [29]. For sum frequency generation in a waveguide, the Stanford group derived an expression for internal up-conversion efficiency [30,31]. In this case, the SFG fields E_p, E_s and E_0 can be written as $E_j(x, y, z) = A_j(z)E_j(x, y)\exp(-i\beta_j z)$, where A_j is the amplitude with the subscript $j = p$ for pump, $j = s$ for signal and $j = o$ for sum frequency output, and $\omega_p = \omega_s + \omega_o$. The above coupled-mode equations (4a)–(4c) can be rewritten using the amplitudes as variants. Since an up-conversion device is always operated in the small signal condition where $A_s \ll A_p$, the pump intensity is non-depleted (i.e. $dA_p/dz = 0$) during the process. If the propagation losses are negligible, at zero phase mismatching these equations can be solved analytically when applying the boundary conditions $A_s(0) = \sqrt{P_s(0)}$, $A_p(0) = \sqrt{P_p}$, and $A_o(0) = 0$, where P_s and P_p are the intensity (power in the waveguide) for the signal and the pump, respectively. Due to the device being used in a photon counting mode; the photon number $N_j = |A_j|^2/(\hbar\omega_j)$ is used in the expression for the conversion efficiency. If we use P_{pump} to represent the pump power before it enters the waveguide, and considering a power coefficient α^2, the power inside the waveguide $P_p = \alpha^2 P_{pump}$. For a waveguide with the length L, we find the solution for the coupled-mode equations:

$$N_o(L) = N_s(0)\sin^2(\alpha \cdot \sqrt{P_{pump}} \cdot L). \tag{10}$$

The internal conversion efficiency is

$$\eta_{int} = \frac{N_o(L)}{N_s(0)} = \sin^2(\alpha \cdot \sqrt{P_{pump}} \cdot L). \tag{11}$$

QPM can remove constraints on finding wavelengths and beam orientations to satisfy phase matching, and allow the highest nonlinear coefficient to be used. For a general comparison, the highest nonlinear coefficient in a lithium niobate crystal is as high as −40 pm/V (d_{33}), whereas the largest coefficient for the birefringent phase-matching in lithium niobate is only −4.64 pm/V (d_{31}). The QPM in PPLN allows us to take advantage of the higher d_{33} nonlinear coefficient. In addition, the QPM technique eliminates the walk-off effect and subsequently, a longer interaction distance within the crystal can be achieved. In this case, it is possible to build a waveguide in the crystal for all three beams to interact. Therefore, higher pump and signal intensities with a longer interaction distance lead to significantly higher conversion efficiencies, which allow us to convert even a single photon. Currently, PPLN waveguides are the most suitable devices to implement single photon frequency up-conversion with almost 100% internal conversion efficiency achievable with relatively low noise.

2.2. Single photon frequency up-conversion detector

Based on QPM frequency conversion technology, we implemented an up-conversion single photon detector. The configuration of this detector is shown in Fig. 2. A 1550-nm continuous wave (CW) laser provides a pump seed. If needed, the seed light can be modulated to an optical pulse train by a synchronized electrical pulse signal. This feature is similar to an optical gate, which is very useful for noise reduction or a high speed gating operation in a communications system. The seed light is then amplified by an erbium-doped fiber amplifier (EDFA). Two 1310/1550 wavelength division multiplexer (WDM) couplers, each with a 25-dB extinction ratio, are used to suppress noise around 1310 nm at the output of the EDFA. The amplified pump light is then combined with a weak signal near 1310 nm by another WDM coupler and the combined pump and signal are then coupled into the PPLN waveguides. The polarization states of both the input signal and the pump are optimized by the polarization controllers, PC1 and PC2, respectively, before entering the coupler. The longer the waveguide, the more interaction length is provided and a lower pump power will be needed to reach the maximum conversion efficiency. The PPLN waveguide used for this up-conversion detector is 5-cm long, which is the longest length possible with current manufacturing capabilities. The input to the PPLN waveguide is fiber coupled, and the output is free-space with a 710-nm anti-reflection (AR) coating. The output light from the PPLN waveguide consists of a 710-nm (SFG) up-converted weak light signal, residual 1550-nm pump light and its second harmonic generation (SHG) at 775 nm. These output beams are separated by two dispersive prisms and the 710-nm photons are detected by a Si-APD. An iris and a 20-nm band-pass filter are used to reduce other noise, such as photons leaked into the Si-APD from the surrounding environment.

Detection efficiency is one of the most important performance metrics for single photon detectors. The overall detection efficiency of an up-conversion detector is determined by the internal conversion efficiency in the PPLN waveguide, the insertion loss due to coupling to the waveguide and at the various components in the system, and the detection efficiency of Si-APD at the converted wavelength. The overall detection efficiency, η_o, of an up-conversion detector can be estimated by the following equation [13]:

$$\eta_o = \eta_{loss} \cdot \eta_{det} \cdot \eta_{con} \approx \eta_{loss} \cdot \eta_{det} \cdot \sin^2(\alpha \cdot \sqrt{P_{pump}} \cdot L) \tag{12}$$

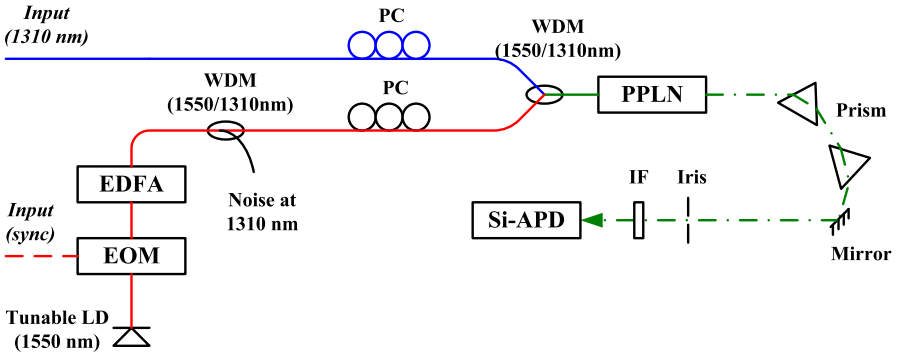

Fig. 2. Schematic diagram of the up-conversion detector. LD: Laser Diode; EOM: Electric-optic modulator; EDFA: Erbium-doped fiber amplifier; WDM: Wavelength-division multiplexing coupler; PC: Polarization controller; PPLN: Periodically-poled $LiNbO_3$ waveguides; IF: Interference filter. Solid line: Optical fiber; Dash line: Free space optical transmission.

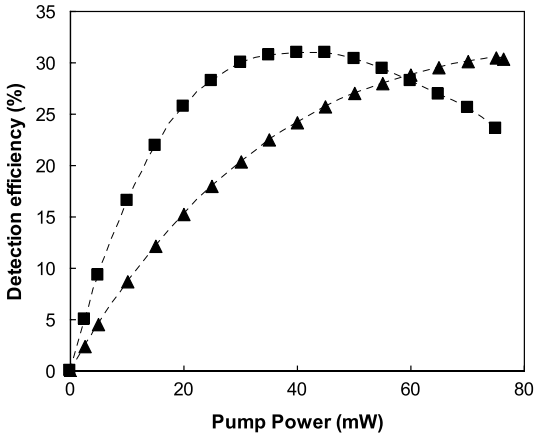

Fig. 3. The detection efficiency as a function of pump power. Two cases are studied: CW pump (triangle) and pulsed pump (square).

where η_{loss} is the total loss in the detector, including the component insertion loss and waveguide coupling loss; η_{con} is the internal conversion efficiency in the PPLN; η_{det} is the intrinsic detection efficiency of the Si-APD at the converted wavelength of 710 nm, and according to the manufacturers' specification is about 65%.

In a complete up-conversion detector unit, the insertion and coupling loss, the detection efficiency of the Si-APD and the structure of the waveguide are fixed. Therefore, the overall conversion efficiency of the detector is determined by the internal conversion efficiency of the waveguide (η_{con}), which is dependent on the pump intensity, and has a $\sin^2(\sqrt{\ })$ relationship according to Eq. (12). The measured conversion efficiency versus the pump power in CW pump mode and in pulsed pump mode is shown in Fig. 3. The measured results are in good agreement with the estimated values from Eq. (12). The maximal detection efficiency is 32% for both pump modes, which corresponds to 100% internal conversion efficiency after we exclude the transmission efficiency due to total insertion loss (η_{loss}, 50%) and the detection efficiency, η_{det}, of the Si-APD (65%). The system efficiency is mostly determined by the losses including waveguide input coupling loss, insertion loss in the waveguide and insertion loss from waveguide output to the Si-APD detector. With a high quality waveguide and very careful arrangement, the highest transmission efficiency of 70% was reported [16], which leads to an overall system efficiency of 46%. When a detector is integrated into a system, more losses will be introduced and therefore, the detection efficiency will be lower. In our case, the PPLN waveguide is fiber pigtailed and therefore the device can be used practically and conveniently in the lab.

In many quantum information systems, such as QKD, the photons arrive with a synchronized classical signal. Therefore, the up-conversion detector can be operated in pulsed pump mode using the synchronized signal. The detection efficiency shown in Fig. 2 is for a pulsed optical quantum signal at 625 MHz with a pulse width of 300 ps (FWHM) pumped by a synchronized classical signal with a pulse width of 600 ps (FWHM). The detector operating in pulsed pump mode can reach the maximum conversion efficiency with a lower average pump power, which helps to reduce the noise (the details are discussed in the next section). In the cases where no synchronized signals exist, a CW pump is needed. For pulsed and CW pump modes, the optimal average pump powers are about 38 mW and 78 mW, respectively. In a pulsed pump mode, the lower optimal average pump power is obtained mainly due to the pulse carving. The above data was taken from our QKD system in which the width of the pump pulse is wider than, and therefore covers, the pulse width of the quantum signal.

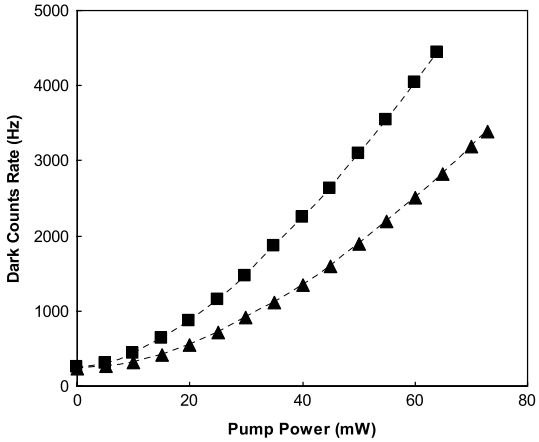

Fig. 4. The dark count rate as a function of pump power at the PPLN input. Two cases are studied: CW pump (triangle) and pulsed pump (square).

When the pulse pump can sufficiently cover the signal pulse, a smaller pump duty cycle will mean that a lower optimal average pump power is required.

The dark count rate, or noise level, is other important performance parameter for single photon detectors: a higher dark count rate can increase errors in a quantum information system and degrade the system's fidelity. Dark counts come from two origins: the intrinsic dark counts of the Si-APD and the noise from the frequency conversion process. The intrinsic dark count rate is dependent on the Si-APD used, which in our case is about 100 counts per second [32]. The noise generated in up-conversion process has been extensively studied [13–18,33], and the main source of the noise is widely believed to be the spontaneous Raman scattering (SRS) and spontaneous parametric down conversion (SPDC) generated in the waveguide by the strong pump. If these SRS photons or SPDC photons are generated at wavelengths within the signal band they can be up-converted to the detection wavelength, generating dark counts not associated with the actual signal. The noise of an up-conversion detector can be reduced by using a pump wavelength that is longer than the signal wavelength, because (1) the anti-Stokes component of the Raman process is much weaker than the Stokes component, and (2) longer wavelength pumps intrinsically avoids generating SPDC photons at the signal wavelength range. A dark count rate of less than 2400 c/s was achieved in our experiment using a pump pulse of 0.6-ns duration within a 1.6-ns total pulse period when the conversion efficiency was maximized.

As shown in the Fig. 4, the pulse pump generates more dark counts than the CW pump for a given average pump power since the peak power of the pulse pump is higher than the average power. We refer to pump power as the average power of the pump, because the pulse pump needs less power than the CW pump to achieve a given detection efficiency. Therefore, the smaller pulse pump power can achieve a given detection efficiency with less dark counts in comparison with higher CW pump. For example, the maximum detection efficiency is reached when using the pulse pump at 38 mW and the dark count rate is 2400 c/s. For the CW pump, a power of 78 mW is needed to achieve the maximum detection efficiency, which incurs a dark count rate of 3100 c/s. Consequently, a pulse pump can use lower power and effectively reduce the final dark count rate compared to a CW pump.

Recently, a long-wavelength pumped up-conversion detector for single photons at 1550 nm was demonstrated in a NIST and Stanford collaboration [34]. A 52-mm long PPLN waveguide was designed for converting single photons at 1550 nm to 843 nm by a tunable pump near 1800 nm generated from a monolithic optical parametric oscillator. This device achieved a total system photon detection efficiency of 37%.

2.3. Frequency up-conversion spectrometer

When the QPM condition in a PPLN waveguide is satisfied at a particular signal wavelength, the maximum up-conversion efficiency is achieved. When the signal is shifted away from that peak wavelength the up-conversion efficiency is reduced, implying that the up-conversion process is wavelength sensitive. In other words, only the photons within the narrow wavelength range, known as the acceptance spectral linewidth, that satisfies the phase matching conditions will experience conversion and be detected. This is similar to a narrow band pass filter, which helps to filter out noise at wavelengths other than the signal wavelength. The acceptance spectral linewidth of the up-conversion detector is determined by the transfer function response of the PPLN waveguide. The transfer function response of a finite-length uniform QPM grating in the waveguide is a function of $\mathrm{sinc}^2(\,)$ as follows [30]:

$$I_o(\Delta k_Q) \propto I_p \cdot I_s \cdot \mathrm{sinc}^2(A \cdot \Delta k_Q \cdot L) \tag{13}$$

where I_o, I_p, I_s are the intensities of the SFG, pump, and signal beams respectively; A is a constant; L is the waveguide length; and Δk_Q is the phase-mismatch. The phase-mismatch in Eq. (13) can be calculated by the following relation with the system

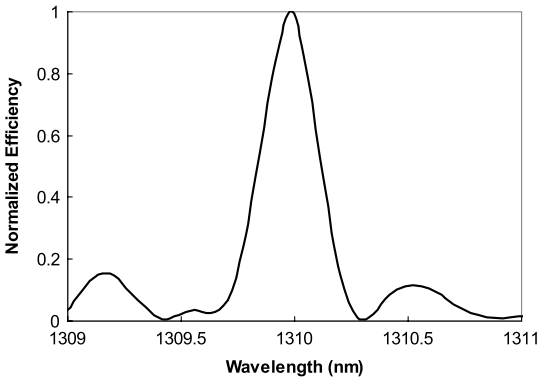

Fig. 5. The normalized detection efficiency as a function of signal wavelength, when the pump wavelength and temperature of the waveguide are fixed.

wavelengths:

$$\Delta k_Q = \frac{n_o}{\lambda_o} - \frac{n_p}{\lambda_p} - \frac{n_s}{\lambda_s} - \frac{m}{\Lambda} \tag{14}$$

where λ_o, λ_p and λ_s are the wavelengths for the output, pump, and signal respectively; and n_o, n_p and n_s are the reflective indices of the crystal for these three wavelengths. Λ is the poling period for the mth order quasi-phase matched condition of the nonlinear PPLN waveguide. According to Eq. (13), the acceptance spectral width is dependent on the length of the waveguide. A longer waveguide will result in a narrower acceptance spectral width. Fig. 5 shows the measured detection efficiency as a function of the signal wavelength at a certain fixed pump wavelength and temperature for our 5-cm long PPLN waveguide. From the figure, we can see that the spectrum is similar to the $\mathrm{sinc}^2(\,)$ function and the acceptance spectral width of the main peak is about 0.2 nm (FWHM). If we use a shorter waveguide or a pump light with a wider spectrum, the acceptance spectral width can be broadened.

Spectrum analysis is important for quantum information research, such as for the study of the spectra of entangled photon sources. For light at UV, visible and wavelengths shorter than 1μm, there are many choices for single photon spectrum analysis with excellent performance based on Si-APDs. One can use either dispersive elements or a tunable narrow-band filter to select light at different wavelengths, which can then be suitably detected by a Si-APD. However, as we have discussed, there are no suitable detectors for the NIR range. The current IR spectrometer technology either has high noise characteristics (in the case of non-cooling InGaAs array detectors), which limits its sensitivity, or needs a bulky cryogenic cooling system (in the case of liquid-nitrogen-cooled InGaAs array detectors).

A NIR spectrometer can be built using an up-conversion detector. In an up-conversion detector, only those photons whose momentum and energy conservation requirements are satisfied with the phase-matching condition in the waveguide can be converted and detected. Based on this principle, an up-conversion spectrometer can be constructed using a tunable pump source [19,35]. In this case, we can measure spectra of weak signals at the single photon power level without using dispersive elements or tunable narrow-band filters.

Based on the up-conversion detector described earlier, we have implemented such an up-conversion spectrometer [19], as shown in Fig. 6. The pump light is provided by a computer controlled tunable CW laser near 1550 nm. The computer scans the wavelength of the 1550-nm pump laser and collects and processes the subsequent counts from the Si-APD. The result is a spectrum of signal light at a single photon power level.

The resolution of the up-conversion spectrometer is jointly determined by the acceptance bandwidth of the PPLN waveguide and the linewidth of the tunable laser. As described earlier, the longer the QPM structure (waveguide), the narrower the acceptance bandwidth. In our case, using a 5-cm PPLN waveguide, the measured acceptance bandwidth is 0.2 nm. Because the linewidth of the 1550-nm tunable laser is as narrow as just 150 kHz, the up-conversion spectrometer resolution is determined by the QPM acceptance bandwidth of the waveguide. A longer waveguide will increase the resolution of the up-conversion spectrometer.

For an up-conversion spectrometer, the sensitivity is jointly limited by the detection efficiency and the deviation of the dark counts in the detector. Our measured maximum overall detection efficiency is 32%. The dark counts show a shot noise behavior, whose deviation is equal to the square root of the average number of the counts. The dark count rate at the maximum detection efficiency in the measurement range is about 2500 counts per second, and the dark count deviation is 50 counts per second. To get a reliable spectrum, the signal counts should be one order of magnitude greater than the dark count deviation, or 500 counts per second, which corresponds to 1563 input photons per second (at 32% detection efficiency), or equivalently −126 dBm, which is at least three orders of magnitude better than current commercial optical spectrum analyzers in the NIR range.

When a Si-APD is used to detect an optical signal at single photon power level, the maximum detection rate is limited by the so called "dead-time" of the Si-APD. After the Si-APD receives a photon, the avalanche process generates an electrical output signal, and the device then needs a certain amount of time, the "dead time", to recover its initial operation state before

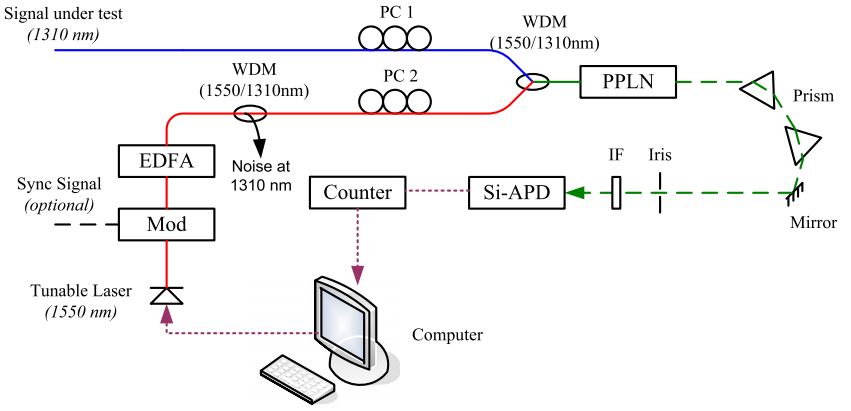

Fig. 6. Schematic diagram of the waveguide-based spectrometer. Mod: Wavelength insensitive modulator; EDFA: Erbium-doped fiber amplifier; WDM: Wavelength-division multiplexing coupler; PC: Polarization controller; PPLN: periodically-poled $LiNbO_3$ waveguides; IF: Interference filter. Solid line: optical fiber; dash line: free space optical transmission; dot line: electrical line.

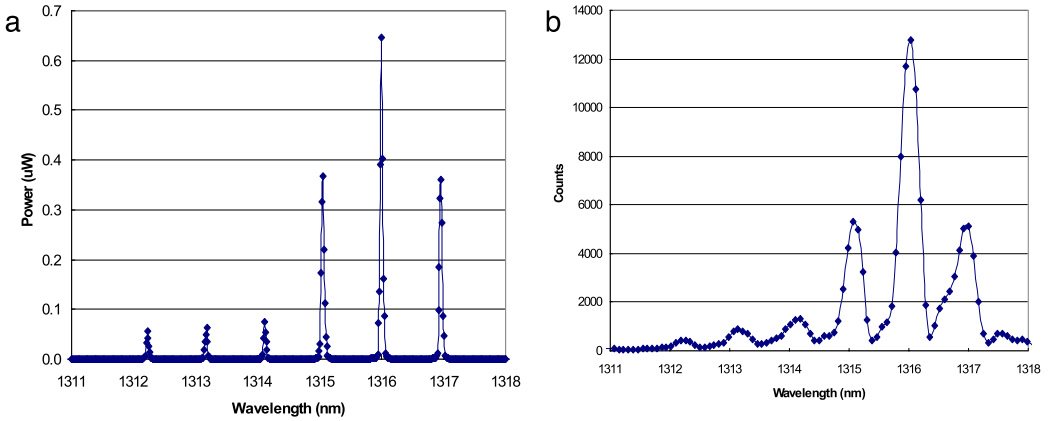

Fig. 7. (a) The spectrum of strong light measured by a commercial OSA. (b) The spectrum of greatly attenuated light measured by the up-conversion spectrometer. The integration time for each measurement point is 500 ms.

detection of the next photon. This is especially significant when the signal intensity becomes high. According to theoretical calculations and experimental data, when the signal intensity is lower than −95 dBm, the influence of the dead-time is negligible. The most suitable measurement intensity range of the spectrometer is therefore from −126 to −95 dBm. If the signal intensity is between −95 and −80 dBm, the influence of the dead time is significant. The measured spectrum should be calibrated to remove the influence of the dead-time and recover the actual spectrum. When the signal intensity is larger than −80 dBm, more than half of the signal photons are lost due to the dead time and, additionally, the Si-APD becomes saturated. Therefore any signal above −80 dBm should be attenuated before using the up-conversion spectrometer.

To demonstrate and verify the functionality of the spectrometer, we used it to measure the longitudinal-mode spectrum of a laser diode. For comparison, an optical spectrum analyzer (OSA, Ando AQ-6315A) was used to record the strong light spectrum, as shown in Fig. 7(a). The spectrum shows one main peak with an amplitude of −33 dBm at 1316 nm, two side peaks (−35 dBm) at 1315 and 1317 nm, and some smaller peaks (less than −40 dBm) between about 1312 and 1314 nm. We then used the up-conversion spectrometer to measure the spectrum of the light after we greatly attenuated it by 75 dB. The scanning range of the pump laser is from 1540 to 1550 nm with a scanning step resolution of 0.1 nm. The integration time at each measurement point is 500 ms. The measured six peaks are clearly shown in Fig. 7(b). The power of all six peaks is less than −110 dBm and the power of the smallest peak is as weak as about −120 dBm. The total time used to record this spectrum was about 1 min. This experiment demonstrates the ultra-high sensitivity of the up-conversion spectrometer. The resolution of the up-conversion spectrometer is limited by the acceptance spectral linewidth as determined by the QPM condition, which can be improved by increasing the length of the waveguide.

The up-conversion spectrometer is a very useful tool for measuring the spectra of weak optical signals at single photon power levels. We have used it to measure the spectra of entangled photon sources developed in our lab at NIST. Fig. 8 shows the spectra of the photons generated by SPDC in 1-cm long and 2-cm long PPKTP waveguides. It shows that the longer the waveguide length, the narrower the spectrum of generated photons. Because the resolution of the up-conversion spectrometer is much greater than the spectrum of photons generated from SPDC, and since the intensity of the photons is

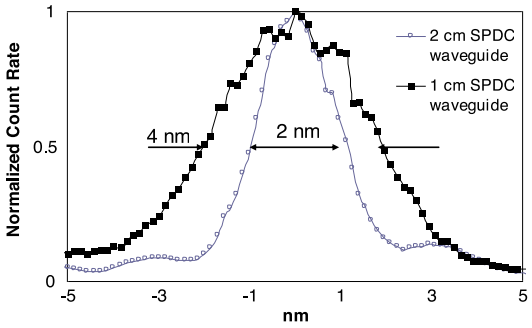

Fig. 8. The spectra of 1310-nm photons generated from 1-cm and 2-cm long PPKTP waveguides, as measured by the up-conversion spectrometer.

quite low and require a highly sensitive device for detection, the up-conversion spectrometer is the most suitable spectrum measurement tool for quantum information research in the NIR range.

3. Applications of single photon frequency up-conversion

3.1. Implementation of quantum key distribution systems

A single photon detector is one of the key elements for a QKD system since the information being transmitted is encoded as the quantum state of single photons [36]. Up-conversion detectors are suitable devices for polarization-based QKD systems because of the following advantages:

1. High detection efficiency: many QKD systems use narrow linewidth attenuated laser light as the single photon source, which is much narrower than the acceptance bandwidth of up-conversion detection. Therefore, an up-conversion detector can convert the entire signal linewidth and thus reach its maximum detection efficiency. This results in a higher secure key rate for the QKD system.
2. Low dark count rate: many QKD systems recover the clock signal from their classical channel. The recovered clock signal can be used as a synchronized trigger for pulse pump operations in the up-conversion detector. Pulsed pumping operation allows lower average power and thus incurs lower dark counts, resulting in a lower error rate in the system.
3. Narrow acceptance spectral bandwidth: each up-conversion detector has a relatively narrow acceptance spectral bandwidth that functions as a band-pass filter. This type of band-pass filter rejects noise such as the crosstalk from strong signals in the classical channel that share the same fiber with the quantum channel.
4. Polarization sensitivity: The up-conversion detector functions as a polarizer required for QKD, eliminating the need for an additional external polarizer and its associated losses.

We integrated our up-conversion detectors into our B92 protocol [37] quantum key distribution (QKD) system using photons at 1310 nm [20]. A QKD system is a point-to-point system that consists of a sender, commonly called Alice, and a receiver, commonly called Bob, who generate a shared secret from quantum measurements for secure communication. The QKD system, as shown in Fig. 9, uses a pair of custom circuit boards with a field-programmable gate array (FPGA) [38–40] to generate and record a random stream of data through the quantum channel and to transmit and receive the classical data through the classical channel. At Alice, 1310-nm CW light is modulated into a 625-MHz pulse train, then randomly polarization encoded and evenly split into two polarization channels. Each pulse train is further modulated by one of two complementary 625-Mbit/s quantum data streams. The two quantum streams are combined by a 45-degree polarization-maintaining combiner and attenuated to a mean photon number of 0.1 per bit, and then wavelength multiplexed with the classical channel and transmitted through a standard single-mode fiber. At Bob, another WDM is used to demultiplex the quantum and classical channels. The quantum channel is polarization-decoded and detected using the up-conversion single-photon detectors, and the detection events are recorded to generate raw keys. Bob and Alice's boards exchange information about the location of the detection events via the classical channel to form a common length key, called the sifted key. Due to noise and possible eavesdropping, Bob and Alice's key's differ. The rate of these differences in the keys is called the Quantum Bit Error Rate (QBER). The QBER is used to guide the final stages of the QKD protocol. Following these final stages, including reconciliation, error correction and privacy amplification, Alice and Bob obtain a common version of their shared secret keys.

The performance of the QKD system is shown in Fig. 10. During our measurements, the pump power was fixed at 40 mW. The sifted-key rate achieved was 2.5 Mbit/s for a back-to-back connection (0 km), 1 Mbit/s at 10 km, and 60 Kbit/s at 50 km. The quantum bit error rate (QBER) is approximately 3% for the back-to-back configuration, remains below 4% up to 20 km, and reaches 8% at 50 km. The finite extinction ratio of the modulator and the system timing jitter induce a background QBER of approximately 2.5% while the remainder comes from dark counts generated by both the pump light and the classical channel. We also calculated the theoretical sifted-key rate and QBER and they agree with the measured results. Although we fixed the pump power close to the maximum up-conversion efficiency, the QBER remains small below 20 km due to the

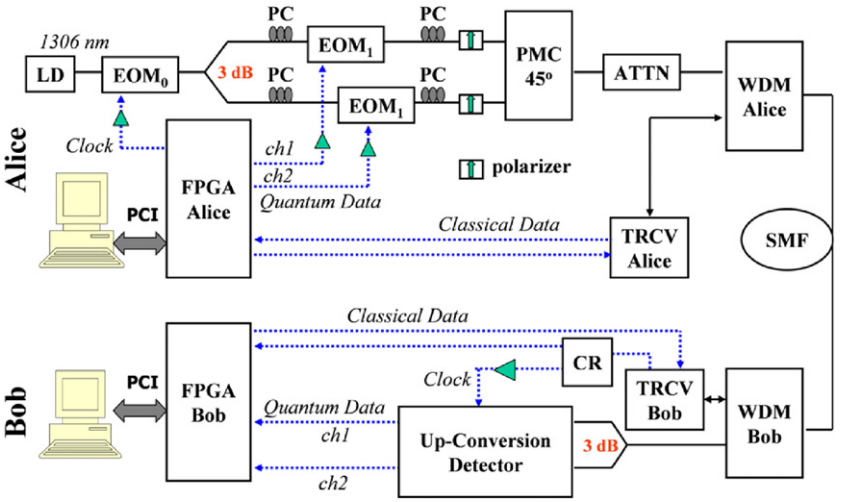

Fig. 9. NISTs B92 polarization encoded QKD system. LD: Laser diode; EOM: Electric-optic modulator ($LiNbO_3$); PC: Polarization controller; PMC-45°: Polarization maintaining combiner that combines two light signals that are separated by 45°; VOA: Variable optical attenuator; WDM: Wavelength-division multiplexer; SMF: Standard single-mode fiber; TRCV: Optical transceiver; CR: Clock recovery module; FPGA: Custom printed circuit board controlled by a field-programmable gate array; PCI: PCI connection; Dotted line: Electric cable; Solid line: Optical fiber.

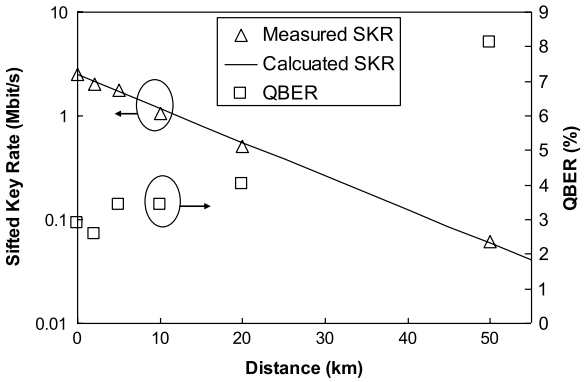

Fig. 10. The sifted key rate and QBER as a function of distance in the NIST B92 polarization-based QKD system.

low dark count rate of the up-conversion detector. The QKD system can generate secure keys in real time for one-time-pad encryption of continuous 200-Kbit/s encrypted streaming video signal transmitting over 10 km. The system performance demonstrates that the up-conversion detectors are suitable for the fiber-based polarization-encoded QKD systems.

3.2. Enabling temporal resolution beyond Si-APD timing jitter limitation

In an up-conversion detector using a CW pump, the temporal resolution is determined by the timing jitter of the Si-APD used. The jitter-limited temporal resolution becomes a bottleneck as the transmission rate increases in a quantum communication system (such as QKD). The temporal resolution of an up-conversion detector can be further increased by using a pulsed pump. An up-conversion detector using a short picosecond pulsed pump can be used in an optical sampling technique which was demonstrated for strong light signals in a number of studies [41,42]. Recently, femtosecond optical sampling was demonstrated in an up-conversion system using ultra-short pump pulses at 790 nm [43]. However, these earlier implementations used a single pump wavelength and are not suitable to increase the transmission rate in quantum communication systems because the sampling rate is still limited by the timing resolution of the Si-APD. We proposed an efficient method to increase the data transmission rate beyond the jitter limitation of the Si-APD by using spectrally and temporally distinct pump pulses in our frequency up-conversion detector [44]. To demonstrate the principle, we report an experimental system that supports twice the jitter-limited transmission rate of the Si-APD, and we show that the approach can be extended to support even higher transmission rates.

In many current quantum communication systems, the temporally encoded quantum data can be generated at rates significantly higher than the single-photon detectors can resolve. For example, commercially available mode-locked lasers or optical modulators can easily generate optical pulses shorter than 10 ps, and broadband SPDC sources can readily prepare

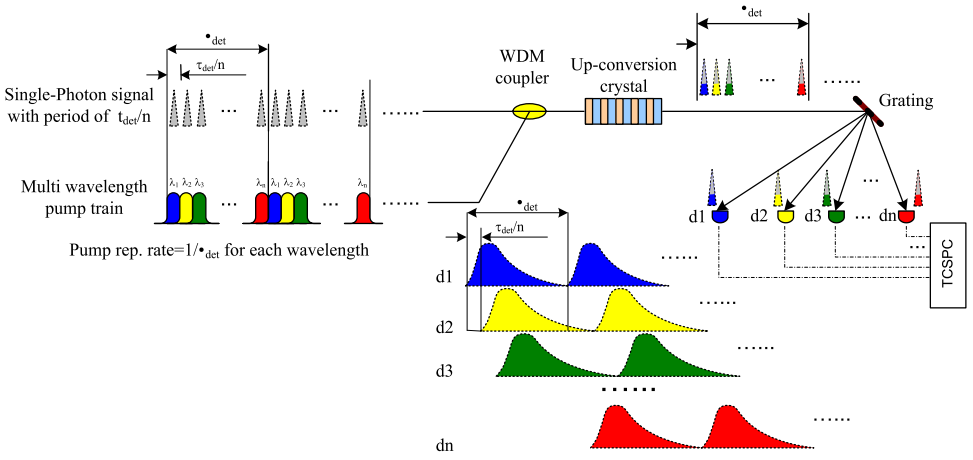

Fig. 11. Schematic diagram of up-conversion single-photon detection with multi-wavelength optical sampling.

correlated photon pairs with sub-100 femtosecond correlation times. On the other hand, current high-resolution single-photon detectors exhibit a full-width-at-half-maximum (FWHM) temporal resolution of the order of 50 ps. In a quantum communication system, insufficient temporal resolution of the detector can cause inter-symbol interference (ISI), i.e., a detection signal can be recorded at a time slot adjacent to the intended one, and this can induce a significant error rate. The transmission rate is therefore limited by the temporal resolution of the single-photon detectors. As a figure of merit, a single-photon signal can be received with an acceptable error rate when the data transmission period is equal to or larger than the full width at 1% of maximum (FW1%M) of the response histogram of the single-photon detector [45]. For most types of Si-APDs the FW1%M is significantly larger than the commonly-cited FWHM. At the peak of a typical Si-APD's temporal response histogram, where the FWHM is measured, the profile is approximately Gaussian, but at lower levels the detector's response deviates significantly from Gaussian, often exhibiting a long exponential tail and this dramatically increases the FW1%M of the device. A typical commercially-available Si-APD has a FWHM of about 350 ps, but a FW1%M of about 1100 ps, which limits the transmission rate to less than 1 GHz for a quantum communication system using an up-conversion detector equipped with this type of Si-APD.

To increase the temporal resolution of an up-conversion detector beyond the jitter limitation of Si-APDs, a multi-wavelength pump and multiple Si-APDs can be used, as illustrated in Fig. 11. A sequence of n pump pulses with different wavelengths are used to sub-divide the Si-APDs minimum resolvable time period, τ_{det}, into intervals of duration τ_{det}/n. Each pump pulse, at a specific wavelength, samples the incident signal in the corresponding interval. To ensure optimum detection efficiency, we consider a pulsed single-photon signal and prepare each pump pulse with a width larger than the single-photon signal pulses. The repetition rate for each particular wavelength of the pump is $1/\tau_{det}$. During one interval, a signal photon enters and co-propagates with one of the strong pump pulses in a quasi-phase matched sum-frequency crystal, such as PPLN, and it can be up-converted to the visible range. During the next interval, another signal photon will co-propagate with a pump photon at a slightly different wavelength than the pump photon in the previous interval and will therefore be up-converted to a slightly different visible light wavelength. The n pump wavelengths produce up-converted photons at n different visible wavelengths during n intervals. Subsequently, the up-converted photons can be separated by dispersive elements such as prisms and distributed to an array of Si-APDs. Each Si-APD in the array therefore corresponds to a particular visible wavelength (as determined by the pump wavelength), and therefore, to a particular arrival time interval of duration τ_{det}/n. In such a configuration, the sampling period for each Si-APD is τ_{det}, allowing it to accurately resolve the signal without ambiguity. The recorded signals can then be recovered into the time domain with a time resolution as small as τ_{det}/n, representing an increase by a factor of n. In this case, a volume Bragg grating can be used to separate the converted photons at different wavelengths without extra losses being introduced. When the device is used as a switch, i.e. only one of the pump beams is turned on at a time, principally the channel number, n, can be very high. When the device is used as a de-multiplexer, in which all pump beams are turned on simultaneously, the channel number n may be limited by the damage threshold of the nonlinear material used.

To experimentally demonstrate the scheme described above, we implemented an up-conversion detector with two pump wavelengths ($n = 2$) and a single-photon signal whose period is significantly less than the FW1%M of the temporal resolution of the Si-APDs used in the system, as shown schematically in Fig. 12. Similar to our previous work [15,16,32], the up-conversion detector is designed to detect signal photons near 1310 nm produced by an attenuated CW laser diode and an electro-optic modulator (EOM) driven by a pattern generator (Tektronix DTG5274). This pulse-carving source produces weak coherent 220-ps (FWHM) pulses with a period of 625 ps (1.6 GHz).

As shown in Fig. 12, the pattern generator also drives pulse-carving systems for the two up-conversion pump seed sources at 1549.2 nm (New Focus 6328) and 1550.0 nm (Agilent 81689A). Each pump seed has a period of 1.25 ns. The pulses from the first pump seed are aligned with the odd signal pulses, while the pulses from the second pump seed are aligned with the

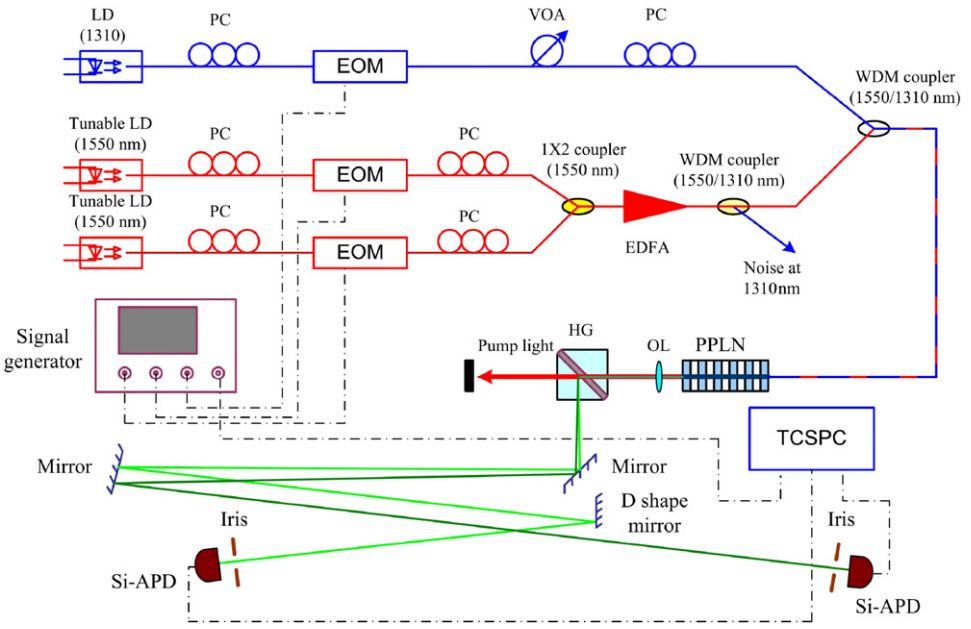

Fig. 12. Experimental setup. LD: Laser diode, EOM: Electric-optic modulator; EDFA: Erbium-doped fiber amplifier; WDM: Wavelength-division multiplexing coupler; PC: Polarization controller; PPLN: Periodically-poled $LiNbO_3$ waveguides; OL, Objective lens; HG, Holographic grating. TCSPC: time-correlated single photon counting.

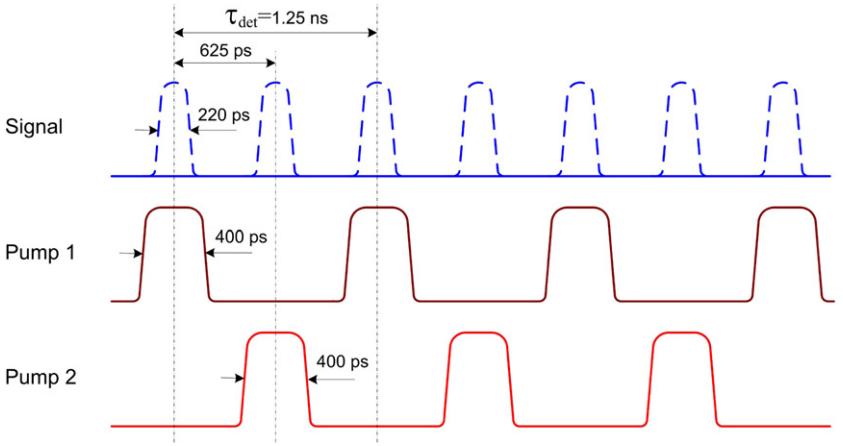

Fig. 13. Timing diagram of the signal (blue), pump 1 (brown) and pump 2 (red) used in the multi-wavelength optical sampling single-photon detection system. (For interpretation of the references to colour in this figure legend, the reader is referred to the web version of this article.)

even signal pulses, as shown as in Fig. 13. The pump-pulse duration used in the experiment is 400 ps, which is wider than the signal pulse and chosen to provide higher conversion efficiency. The two pump seed beams are combined by a 1×2 coupler and then amplified by a 1-Watt erbium-doped fiber amplifier (EDFA) (IPG Photonics: EAR-0.5K-C). Two 1310/1550 WDM couplers are used in series at the output of the EDFA to provide a 50-dB extinction ratio in order to remove amplifier noise around 1310 nm. The amplified pump light is then combined with the 1310-nm signal by another WDM coupler, and together they are coupled into the up-conversion crystal. In this experiment, up-conversion takes place in a 1-cm PPLN waveguide (AdvR Inc.) that has a fiber-coupled input and a free-space output. When mixed with the slightly different pump wavelengths in the PPLN waveguide, the 1310-nm signal photons are up-converted to output photons at 710.0 and 709.8 nm. The output beam is filtered to remove noise and excess pump light and then diffracted by a holographic grating (Kaiser Optical Systems, HLBF-710). After a 3-m path, the 710.0-nm and 709.8-nm photons are sufficiently separated such that they can be directed onto two Si-APDs (PerkinElmer SPCM-AQR-14). In this system, an adjustable iris is placed in front of the Si-APD, and in conjunction with the holographic grating, acts as a 0.4-nm band-pass filter which greatly reduces the dark count rate. The detected signals are counted by a time correlated single photon counter (TCSPC).

For a quantum communication system, the inter-symbol interference (ISI) can be a significant source of errors [46]. ISI can be caused by the timing jitter of the single photon detectors, and in order to avoid a high bit-error rate, the transmission

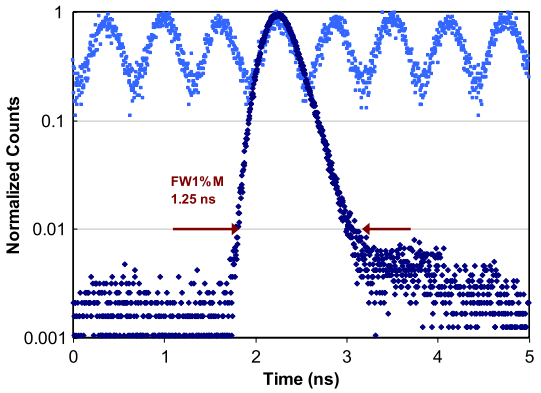

Fig. 14. Response histogram of the up-conversion detector with a single pump wavelength. The response histogram of single pulse (dark blue) shows the FW1%M is 1.25 ns and its temporal resolution is insufficient to resolve, with low ISI, the repetitive data pattern "11111111" at 1.6 GHz (light blue). (For interpretation of the references to colour in this figure legend, the reader is referred to the web version of this article.)

data cycle should be equal to or larger than the FW1%M of the response histogram, thus limiting the data rate. For the 220-ps signal pulse used in our system, the response histogram of an up-conversion detector with a single wavelength pump is shown in Fig. 14 (dark blue lower trace). The FW1%M of the histogram is about 1.25 ns and this detection system can therefore support a transmission rate of 800 MHz. When such a detection system is used to detect a 1.6-GHz signal, severe ISI occurs due to the detectors insufficient temporal resolution as indicated by the poor pulse resolution shown in Fig. 14 (light blue upper trace). As described above, we implemented an up-conversion system in which two pumps at slightly different wavelengths are alternatively applied and the photons converted to two different wavelengths are separated by a dispersive element and detected by two Si-APDs, APD 1 and APD 2. APD 1 receives the signal at odd time bins and APD2 receives the signal at even time bins. The FW1%M of the response histogram for each pump wavelength channel is 1.25 ns, corresponding to a transmission rate of 800 MHz. However, the whole system consisting of two channels supports an overall transmission rate of 1.6 GHz. Fig. 15 (a) shows the response histogram of each Si-APD in the optical-sampling up-conversion system for a repetitive signal pattern "11111111". For each APD, the detection window is larger than the FW1%M of the APD response, so the ISI is negligible. To illustrate both the temporal demultiplexing and the ISI in this system, Fig. 15 (b) shows the response histograms of APD 1 and APD 2 for a repetitive signal pattern "10010110". APD 1 receives the signal at odd time bins, resulting in the pattern "1001", and APD 2 receives the signal at even time bins, resulting in the pattern "0110", and the original signal can be reconstructed from the data recorded by the two APDs. To measure the error rate caused by the ISI in the optical sampling up-conversion system under conditions similar to a QKD system, we directly generated an original signal data using a 1.6-GHz pseudo-random data pattern and then compared the measured data to the original data. The error rate was found to be approximately 1.2%. Subtracting the error rate caused by the imperfect extinction ratio of the modulator and the intrinsic dark counts of the APDs, the error rate caused by ISI is less than 1%.

The internal conversion efficiency and QPM bandwidth of the conversion device are related to its length according to Eqs. (11) and (13), respectively — a shorter device will provide a broader less efficient conversion. The conversion device used in this experiment was a 1-cm long PPLN waveguide. The QPM acceptance bandwidth is broad enough to contain two frequency conversion channels, accepting two pump wavelengths separated by only 0.8 nm. In order to use both pump wavelengths, they are each tuned to either side of the QPM acceptance bandwidth peak. The conversion efficiency of the device is therefore lower in comparison with that of traditional one-channel devices when the pump wavelength is optimized at the QPM peak. In addition, the lower conversion efficiency is due to the shorter waveguide used. To overcome these difficulties, it is possible to design a special dual-channel up-conversion device, in which either of two pump wavelengths can be used to optimally convert photons from a signal wavelength to one of two SFG wavelengths in the corresponding channel. In Section 2.1, Eq. (7) describes the mth Fourier component of the nonlinear coefficient. For a PPLN structure, all adjacent domains are uniformly poled in opposite direction with the same length l or with a constant period Λ. Thus, for a traditional single channel device, we can simply set $D = l/\Lambda = 1/2$. In a more general case, the domain length l changes as a periodic function of z. In another words, the phase of the domain length l is periodically modulated with a phase-modulation period Λ_{ph} [47]. In this case, the nonlinear coefficient can be expressed using a phase-modulation function. From the Fourier transform analysis, we found that the phase-modulated grating of the nonlinear coefficient provides multiple QPM peaks when the wave-vector mismatch satisfies the equation:

$$\Delta k_Q = k_o - k_s - k_p - 2\pi\left(\frac{1}{\Lambda} + \frac{m}{\Lambda_{ph}}\right), \tag{15}$$

where m is the order number of the Fourier components. We are able to design an up-conversion device with multiple QPM peaks. The wavelength interval between two adjacent peaks is determined by the phase-modulation period Λ_{ph}. Such a new device can resolve the difficulties of low conversion efficiency of the shorter device used in our experiment. In particular,

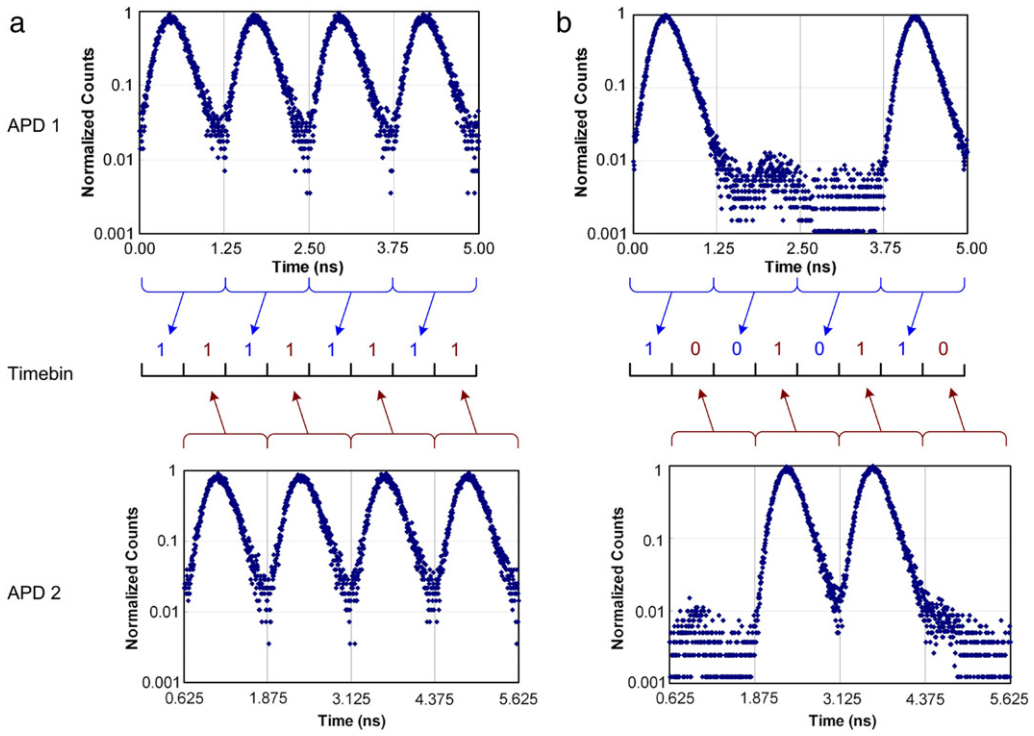

Fig. 15. Response histogram of the up-conversion detector with two spectrally and temporally distinct pump pulses (a) response histograms of APD 1 and APD 2, for a repetitive signal pattern "11111111" at 1.6 GHz. (b) response histograms of APD 1 and APD 2, for a repetitive data pattern 10010110 at 1.6 GHz.

dual-channel (corresponding to $m = \pm 1$) up-conversion devices are currently being studied in the lab. The dual-channel or multi-channel up-conversion devices will open up many new applications in the future.

3.3. Characterization of an entangled photon source

Entangled photon pair sources are one of the most important tools for the realization of complex quantum communication protocols, such as quantum teleportation or entanglement swapping. For fiber-based quantum communication systems, time-bin entanglement is more suitable than polarization entanglement since it is not sensitive to polarization changes in optical fibers. The original time-bin entanglement approach is realized using consecutive laser pulses generated by an unbalanced interferometer to pump a nonlinear media. During the process, the two pulses have a certain probability to generate a photon pair by SPDC and produce time-bin entangled photon pairs [48,49]. When a laser pulse train is used to pump the nonlinear media, and the condition $T_c \gg \tau \gg \tau_p$ (where T_c is the coherence time of the pump beam, τ is the pulse interval, τ_p is the pulse duration) is satisfied, sequential time-bin entanglement can be generated [50–52]. The sequential time-bin entanglement scheme does not need an interferometer at the source, and can achieve high-repetition rates which are more suitable for quantum communication.

For a fiber-based system, it is desirable to use a non-degenerate entangled photon pair, in which the wavelength of one photon is in the telecom band, and the other one is resonant with an atomic transition suitable for quantum memory. We implemented a sequential time-bin entangled photon source by using a periodically poled potassium titanyl phosphate (KTP) waveguide [22]. In this entangled photon source, one photon at 1310 nm is suitable for long range fiber communications; and can be detected by our up-conversion detector. The other photon at 895 nm is resonant with the D1 transition line of cesium (Cs) atoms. Cs atoms are a good candidate for building quantum memory.

Fig. 16 schematically shows the experimental setup. A CW tunable laser (New Focus: TLB 6321) emits a narrow linewidth (300 kHz) coherent beam with a coherence time $T_c = 3.3\ \mu$s which is modulated by an electric-optic modulator (EOM) at a repetition rate of 1 GHz (pulse duration $\tau = 1$ ns) and a pulse interval $\tau_p = 330$ ps (FWHM). In this case, the coherence time is greater than the pulse duration, which in turn is greater than the pulse interval, thus satisfying the requirement for generating sequential time-bin entangled photon pairs. Simultaneously, another channel in the pulse generator provides a 1-GHz pulse train with a FWHM of 500 ps to the up-conversion detector for pulsed pumping, and the time delay between the two channels is adjustable. The 1064-nm optical pulses are further amplified by a fiber amplifier (IPG: YAR-1K-LP). A polarization controller (PC) is used to launch the proper polarization into the first PPKTP waveguide, which is used to

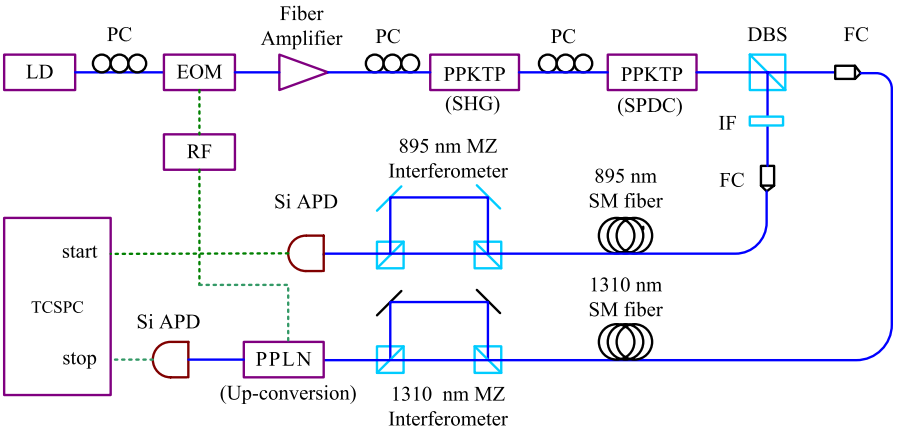

Fig. 16. Experimental setup. LD: 1064-nm CW laser diode; EOM: Electric-optic modulator; RF: RF pulse generator; PC: Polarization controller, PPKTP: Periodically-poled KTP waveguide; DBS: 895-nm and 1310-nm dichroic beam splitter; IF: Interference filter; FC: Fiber collimator; MZI: Mach–Zehnder interferometer; Si-APD: Silicon based avalanche photodiode; PPLN: Periodically-poled $LiNbO_3$ waveguide for frequency up-conversion; TCSPC: Time-correlated single photon counting module. Solid line: Optical path; Dash line: Electrical connection.

generate 532-nm pump pulses by SHG. The pump pulses are then coupled into a 532-nm single-mode fiber, which removes the 1064-nm light and other noise from the fiber amplifier before entering into the second PPKTP waveguide.

A series of time correlated pairs, consisting of photons at 1310 and 895 nm, are generated in the second PPKTP waveguide. Both emerging photons and the pump are vertically polarized with type 0 phase matching. By adjusting the pump power, an average of 1 pair of SPDC photons per N pump pulses is generated. Under the condition of $N \gg 2$ and $T_c \gg \tau \gg \tau_p$, the quantum state of the photon pair is:

$$|\Psi\rangle = \frac{1}{\sqrt{N}} \sum_{n=0}^{N-1} e^{in\phi_\tau} |\tau\rangle_{signal} |n\tau\rangle_{idler} \tag{16}$$

where ϕ_τ is the phase difference between consecutive pump pulses; i is the imaginary unit; and the subscripts signal and idler represent the signal (895 nm) and idler (1310 nm) photons. The signal and idler photons are separated using a dichroic beam splitter, and then coupled into 895-nm and 1310-nm single mode fibers, respectively. A bandpass filter is used to reduce the residual pump photons and other noise in the 895-nm photon path, while the noise in the 1310-nm path will be filtered by the up-conversion detector, as described earlier. To measure the two-photon-interference-fringe visibility, Franson type interferometers are used [53]. We built two free-space unbalanced Mach–Zehnder interferometers (MZIs) with a 1-ns optical path difference for both signal and idler channels. The signal and idler photons are then passed through their own MZI and detected by a Si-APD and an up-conversion detector, respectively. The phase difference of the beams in the two paths in each interferometer is adjusted by a piezo-nano-positioning stage. Due to a variety of optical losses, the classical visibility of the two MZIs is about 18 dB. The visibility can be maintained for more than a half hour in our laboratory environment, which is long enough for our entanglement measurements. Temperature control is needed to achieve longer time stability.

Fig. 17 shows the histogram of coincidence photon pairs with three coincidence peaks. The two side coincidence peaks correspond to when both photons pass through either the long (idler) / short (signal) path or the short (idler) / long (signal) path in the interferometers. In these cases, there is no interference. The central peak records the coincidence counts where both photons pass through the same path, either both long paths, or both short paths. Because the photons in the earlier time bin and those in the later time bin are indistinguishable and the phase difference between two adjacent time bins are constant, photon-pair interference occurs. The interference pattern can be estimated by the following equation [54]:

$$R_c = 1 - V \cos(\theta_s + \theta_i + \phi_\tau) \tag{17}$$

where R_c is the normalized coincidence counting rate at the central peak; V is the visibility of the interference fringes; θ_s and θ_i are the phase difference between long and short paths in the interferometers for the signal and the idler respectively; and ϕ_τ is the phase difference between consecutive pump pulses. The coherence time of the pump is much longer than the optical path time difference of the interferometer, so ϕ_τ is a constant. Thus the interference pattern is determined by the relative phases of the two interferometers $(\theta_s + \theta_i)$.

To determine the two-photon-interference-fringe visibility of the entangled photon pairs, we measured the photon coincidence through the interferometers, in which we fixed the phase for the signal interferometer (895 nm) and varied the phase for the idler interferometer (1310 nm). We set the detection time-window to be 400 ps as an optimal time to maximize counts and minimize noise from adjacent coincidence peaks. To demonstrate entanglement, we set two different fixed phases for the signal and got two interference patterns with the varied phase of the idler, as shown in Fig. 18. For each data point, we took six measurements and then calculated the average value and their standard deviation to determine the

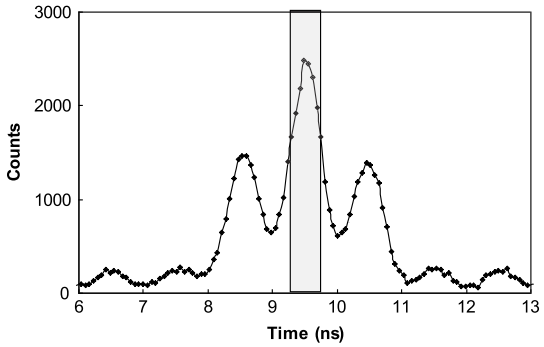

Fig. 17. Histogram of the coincidence counts of photon pairs after the two MZIs. The shaded area indicates the detection window (400 ps). The integration time for each data point is 10 s.

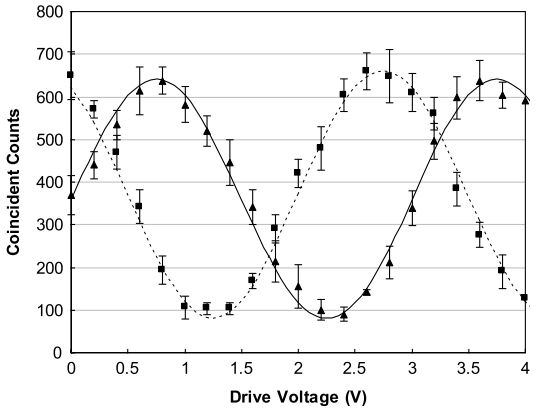

Fig. 18. Coincidence interference fringes measured in the experiments. Solid line/triangle and dash line/square are the coincidence counts when the piezo-drive voltages of the 895-nm interferometer are 0 and 1 V, respectively. The coincidence counts are collected in 400 ps window in a 10 s interval.

error bar. The average visibility of the two curves is 79.4% without subtraction of noise, which is well beyond the 71% visibility for violation of the Bell inequality [55]. The measurement deviation is mainly caused by the temperature fluctuation of the interferometers. The measured visibility can be improved with the use of thermally insulated interferometers and better detectors with lower timing jitter, and if the more recently developed low noise up-conversion detectors were used.

Because the spectral width of the 1310-nm photon generated from SPDC in the PPKTP waveguide is about 2 nm (FWHM), which is much wider than the acceptance bandwidth of the PPLN waveguide (0.2 nm), the detection efficiency of the up-conversion detector is reduced to about 3 % of the photons from that source. However, the narrow bandpass property of the up-conversion detector provides an advantage. We do not need to use any other narrow band pass filter in the 1310-nm optical path, since other wavelengths do not satisfy the QPM condition required for conversion and therefore remain at a wavelength that cannot be detected.

3.4. Characterization of photons from semiconductor quantum dots

In the quantum information research area, semiconductor quantum dots (QD) are widely being studied and utilized as a good resource that provides non-classical, or anti-bunched, single photons. One of the emission wavelength bands for commonly available indium arsenic (InAs) quantum dots is near 1310 nm, where low loss transmission through fiber is possible. That makes the study of photons from QDs more attractive. However, as noted earlier, Si-APDs do not work at this telecommunication band. Transducing non-classical states of photons from one wavelength to another is an important approach for integrating quantum systems at different energies [56,57]. For instance, transducing a single photon source at 1310 nm to the visible part of the spectrum for detection with Si-APDs would be a critical part of a linear optical quantum computation scheme. The up-conversion technique provides a powerful tool for such studies. In this section we will discuss the application of the up-conversion detectors in the investigation of photons from semiconductor QDs.

The experimental setup for the study of single photons from an InAs QD using the up-conversion is shown in Fig. 19. Following the technique of Ref. [58], a fiber taper waveguide (FTW) is used to deliver the excitation source to and collect the photoluminescence (PL) from a cryogenically-cooled single epitaxially-grown InAs QD in a 2.0-μm diameter mesa. The excitation source is a pulsed gain-switched laser diode at 780 nm with 50-MHz repetition rate and a 50-ps pulse interval. This laser is attenuated to 10 nW before being coupled into a 1 μm diameter FTW. The FTW is precisely positioned to contact

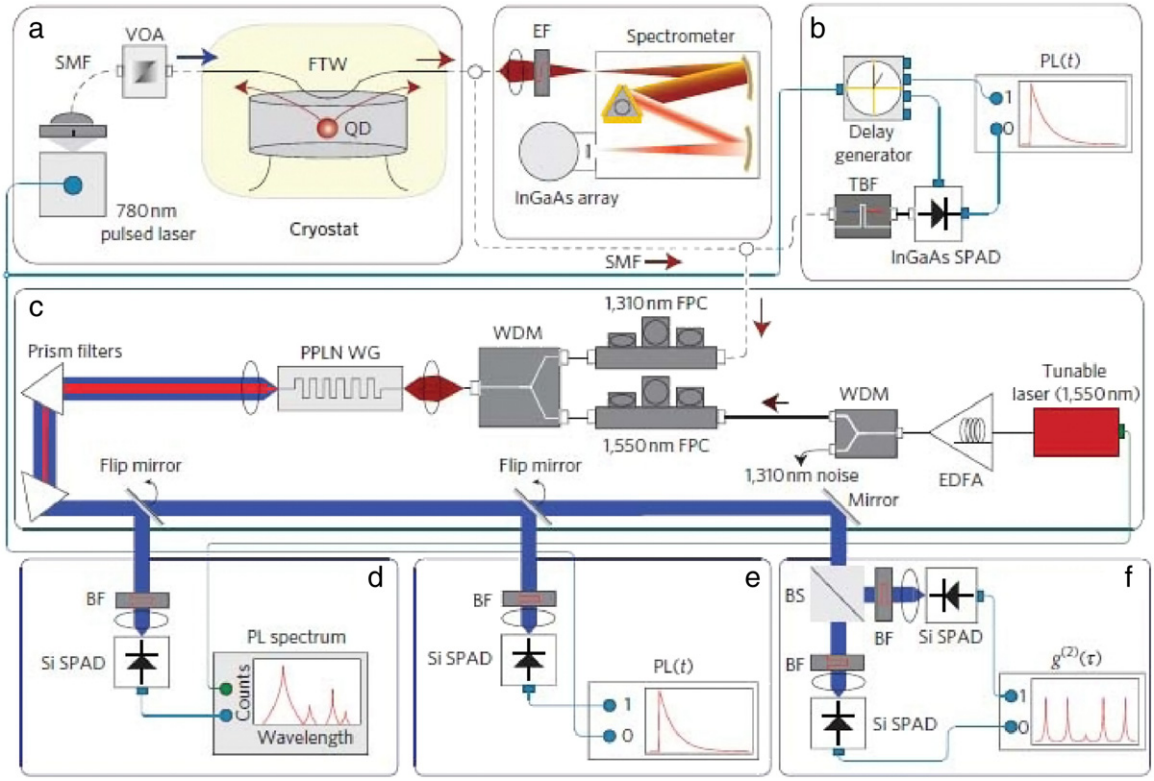

Fig. 19. Experimental schematic for up-conversion of photoluminescence from a quantum dot. (a) Schematic of experimental setup for excitation and collection of quantum dot PL by a FTW. (b) Schematic for time-resolved PL measurement using an InGaAs SPAD. (c) PPLN wavelength conversion part of the experimental setup. (d) Schematic for PL spectroscopy after up-conversion. (e) Schematic for time-resolved PL measurement after up-conversion. (f) Schematic of Hanbury-Brown and Twiss interferometer after up-conversion. PL: Photoluminescence; Si SPAD: Silicon based single photon avalanche photodiode (Si-APD); FTW: Fiber taper waveguide; SMF: Single-mode fiber; VOA: Variable optical attenuator; FPC: Fiber polarization controller; WDM: Wavelength division multiplexer; EDFA: Erbium-doped fiber amplifier; TBF: Tunable bandpass filter; EF: Edge-pass filter; BF: Bandpass filter; BS: Non-polarizing beam splitter; PPLN WG: Periodically poled $LiNbO_3$ waveguide.

with the mesa. The evanescent field of the 780-nm pump laser excites the QD which emits PL photons. A significant fraction of the photons are emitted back into the FTW and then coupled into a single mode fiber. To measure the QD PL spectrum, the PL is coupled into a traditional grating spectrometer equipped with a cooled InGaAs detector array as well as into our up-conversion spectrometer for comparison.

Fig. 20(a) shows a QD PL spectrum recorded by a commercial grating spectrometer over an integration time of 60 s. The sharp lines of a single QD are measured near 1300 nm and are identified to be two different charge states of the same QD. Fig. 20(b) shows the same PL spectrum but recorded using our up-conversion spectrometer over an integration time of only 1 s. To record the spectrum as we described in Section 2.3, the pump laser is spectrally tuned from 1555 to 1556 nm in incremental steps of 0.1 nm, while the output pulses from the APD are counted in 1-s time bins. As shown in Fig. 20(b), the spectral resolution is limited to $\sim$0.2 nm according to the up-conversion phase-matching bandwidth and can be improved with a longer chip. Of more importance to subsequent photon counting measurements is that a similar signal-to-noise ratio is obtained by our up-conversion spectrometer over an integration time that is only 1/60th of the traditional grating spectrometer.

An important counterpart to the aforementioned steady-state spectroscopy is a time-resolved PL measurement, which can reveal the excited-state lifetime of the quantum dot transition and provide insight into effects such as radiative cascades and non-radiative decay. The QD radiative lifetime can be obtained from the slope of the PL decay curve. To record such decay curves, one of the two PL peaks (see Fig. 20) must be filtered out to ensure that only the PL photons from the particular charge state we are interested are characterized. In our case, the peak at 1302.6 nm is filtered by a tunable 1-nm bandpass filter. By incorporating a time-correlated single photon-counter (TCSPC), synchronized with the pulsed excitation laser, the decay curve can be recorded as a histogram of start–stop events as shown in Fig. 21. The decay curve shown in the left side of Fig. 21 is recorded using an InGaAs APD with a 20-ns gate and an integration time of 700 s. The data leads to a lifetime of 1.3 ns $\pm$ 0.1 ns. Fig. 21 (right) shows a similar measurement using our up-conversion detector with an integration time of 600 s. The up-conversion bandwidth is narrow enough to filter out the peak at 1302.6 nm and so no additional bandpass filter is needed. The data measured using our up-conversion detector shows a dynamic range about 25 times better than

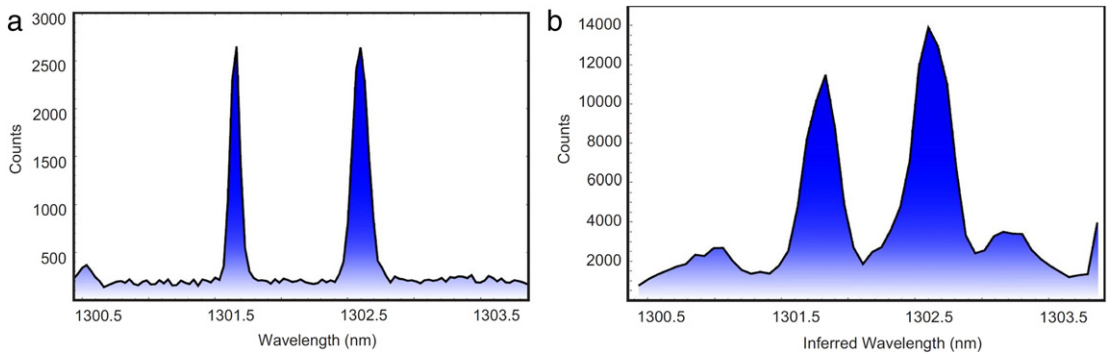

Fig. 20. (a) PL spectrum taken with a grating spectrometer equipped with an InGaAs array over an integration time of 60 s. (b) PL spectrum measured by the up-conversion spectrometer over an integration time of 1 s. The two peaks represent the two different charge states of the same QD.

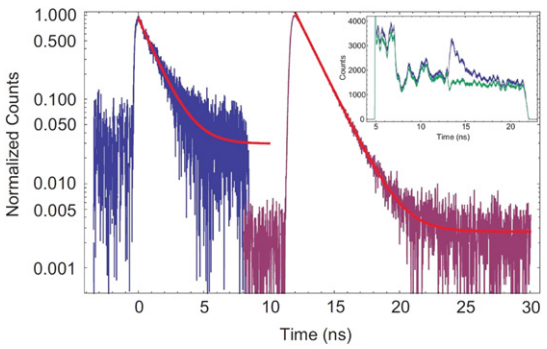

Fig. 21. PL lifetime measured by the InGaAs APD (blue) and the up-conversion detector using a silicon APD (maroon). Inset: raw histograms of the signal (blue) and dark count only (green) traces taken with the InGaAs APD. (For interpretation of the references to colour in this figure legend, the reader is referred to the web version of this article.)

that using the commercial InGaAs APD. As a result, the measurement accuracy is higher as demonstrated with a lifetime of 1.38 ns $\pm$ 0.03 ns.

It is well known that semiconductor QDs provide non-classical, or anti-bunched, single photons. When we use an up-conversion detector to detect the photons, we must convert the wavelength of the photons from the NIR to the near visible range. It is important to know if the non-classical features of the photons from the QD are preserved during the conversion process. To answer this, we measured the second-order correlation $g^{(2)}(\tau)$ function for the up-converted photons at 710 nm using a Hanbury-Brown and Twiss interferometer as depicted in Fig. 18(f). The outputs of the Si-APDs were used as the start and stop signals for the TCSPC. The normalized histogram of such start–stop events is $g^{(2)}(\tau)$ and is shown in Fig. 22. The reduction of the normalized counts at $\tau = 0$ is a clear indication of photon anti-bunching and the non-classical nature of the optical field. The value $g^{(2)}(0)$ can be obtained by comparing counts in the $\tau = 0$ peak to the average of those in the $\tau \neq 0$ peaks. In our experiment, we obtain a value of $g^{(2)}(0) = 0.165 \pm 0.010$. Because of the value $g^{(2)}(0) = 0.165 < 0.5$, the optical field must be dominantly composed of single photons. The non-zero value of $g^{(2)}(0)$ is due to approximately equal contributions from dark counts and background emission at the QD wavelength that are collected by the FTW. The dark counts in our up-conversion detector are dominated by up-conversion of anti-Stokes Raman photons from the pump laser. Another feature of Fig. 21 is that the peaks nearest $\tau = 0$ at $\tau = \pm 20$ ns and $\tau = \pm 40$ ns do not recover completely, even though the quantum dot lifetime is only 1.38 ns. This sub-microsecond correlation effect has been measured previously for quantum dots [59] and is thought to be caused by the preferential capture of single carriers into the quantum dots rather than electron–hole pairs. The strength of this effect is known to depend strongly on excitation wavelength and power.

In this measurement, we have demonstrated that up-conversion can be used for high signal to noise spectrometry and time-correlated photon counting for QD lifetime measurements. Meanwhile, we have also demonstrated that the quantum mechanical nature of the single-photon stream emitted from a QD at 1300 nm is successfully transduced to a 710-nm optical field since the recorded second order intensity correlation function $g^2(\tau)$ is actually measured from the up-converted photons at 710 nm. This experiment shows that the up-conversion detector is suitable for second order photon correlation measurements in the NIR region. Furthermore, in the next section we will show that our up-conversion detectors are capable of more challenging (third and fourth order) photon correlation measurements in the NIR region due to their high conversion efficiency and low dark count rate.

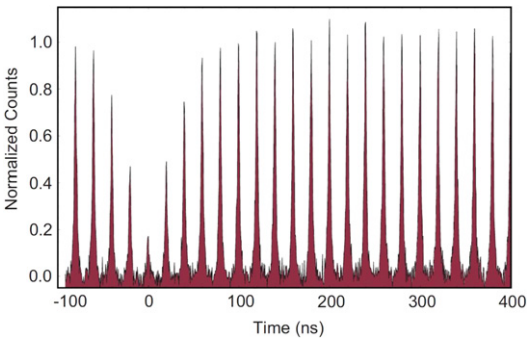

Fig. 22. Normalized second-order intensity correlation $g^{(2)}(\tau)$ after dark count event subtraction.

3.5. Higher-order photon correlation measurements in NIR region

In 1956, Hanbury-Brown and Twiss (HBT) first developed an instrument to record the correlation between photocurrent fluctuations from two far apart photocells when illuminated by a star [60]. This instrument, known as the HBT interferometer, was used to measure the angular diameter of visual stars. Historically, HBT can only record the correlation between fluctuations in the currents, and therefore the light intensities, from the two photocells. The $g^{(2)}(\tau)$ is therefore commonly called the second order intensity correlation. Following on from their pioneering work, photon correlation has been used to study the statistical behavior of the arrival times of photons emitted by a variety of photon sources using advanced photon counting techniques [61]. So $g^{(2)}(\tau)$ is also called the second-order temporal correlation. Recently, higher orders of temporal correlation, e.g. third- and fourth-order temporal correlations ($g^{(3)}(\tau_1, \tau_2)$ and $g^{(4)}(\tau_1, \tau_2, \tau_3)$), have drawn attention, since they can reveal more information about the sources of the photons being characterized. While higher-order correlation measurements can be implemented in the visible range by using highly efficient silicon-based single photon detectors, such as Si-APDs [62], measurements in the NIR range are limited by the lack of commercially available high performance single photon detectors. Recently, higher-order temporal correlation measurements in the NIR range were implemented by using four-element superconducting nanowire single-photon detectors (SNSPDs) [63]. However, the four-element SNSPDs need to work at liquid helium temperatures and are not yet widely available commercially.

As described in Section 3.4, our second order photon correlation proves that the sub-Poissonian statistical nature of the photons from a quantum dot is preserved in the frequency up-conversion process [23], but it is difficult to directly compare the measured results to the theory because the quantum dot is not a perfect single photon source. In this section, we introduce our measurements of higher orders, including second, third and fourth orders of temporal correlation of photons from two well-known types of photons sources: a coherent source (highly attenuated laser) and a pseudo-thermal source [24]. By using the up-conversion device, we convert photons in the NIR region into the visible region, and then measure the temporal correlation (up to the fourth order) of the up-converted photons using Si-APDs with a high detection efficiency. We find that the original photon statistics are preserved in the up-conversion process. Therefore, this approach can be used to study the statistics of photons in the NIR region accurately and efficiently.

The experimental configuration is shown in Fig. 23. As described above, a 5-cm long PPLN waveguide is used to convert signal photons around 1310 nm, to the visible region (710 nm) by a pump beam at 1550 nm. Three half-wave plates (HWPs) and polarizing beam splitters (PBS) for 710 nm are used to split the up-converted photons to be detected by four Si-APDs. A four-channel time-tagged counting system records photon arrival times at each detector. These time-tagged data are post-processed to acquire multi-start and multi-stop correlation histograms between two, three, and four channels, and then the high-order temporal correlations $g^{(2)}(\tau)$, $g^{(3)}(\tau_1, \tau_2)$ and $g^{(4)}(\tau_1, \tau_2, \tau_3)$ are calculated and plotted. To avoid significant influence of noise, the signal photon flux is set at 800k counts/s for both coherent light and pseudo-thermal light, which are two orders of magnitude larger than the noise photon level. In the post-processing, we use 25 ns time bins for calculation and therefore the mean photon number of each time bin is 0.02.

The measured second, third and fourth order temporal correlation values are shown in Fig. 24. For coherent light, the measured data of $g^{(2)}(\tau)$, $g^{(3)}(\tau_1, \tau_2)$ and $g^{(4)}(\tau_1, \tau_2, \tau_3)$ are all close to the expected theoretical value of 1. For the pseudo-thermal source, the data shows that photons are bunched around the origin, with peak values and standard deviations of $g^{(2)}(0) = 2.001 \pm 0.035$, $g^{(3)}(0, 0) = 5.87 \pm 0.23$ and $g^{(4)}(0, 0, 0) = 23.1 \pm 1.9$. The peak values are in good agreement with the theoretical values of $2! = 2$, $3! = 6$ and $4! = 24$, respectively.

In this experiment, the coherent source and pseudo-thermal source are near 1310 nm, while all results for $g^2(\tau)$, $g^3(\tau_1, \tau_2)$ and $g^4(\tau_1, \tau_2, \tau_3)$ are actually measured using the up-converted photons at 710 nm. The temporal correlation results of up-converted photons are in good agreement with the theoretical values and the results from experiments using SNSPDs in Ref. [63]. We conclude that the photon statistics are well preserved in the up-conversion process. Thus, frequency up-conversion is proved to be an accurate, relatively inexpensive, and highly efficient measurement method for temporal correlation of photons in the NIR region.

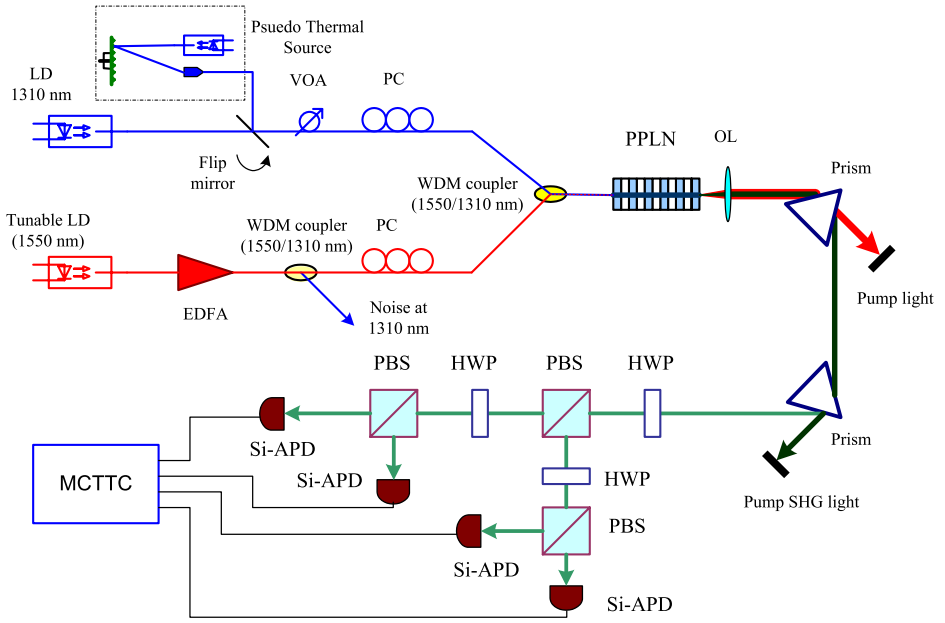

Fig. 23. Schematic diagram of the experimental setup. LD: Laser diode, EDFA: Erbium-doped fiber amplifier; WDM: Wavelength-division multiplexing coupler; PC: Polarization controller; PPLN: Periodically-poled $LiNbO_3$ waveguide; OL, Objective lens; HWP: Half-wave plate; PBS: Polarizing beam-splitter; MCTTC: Multi-channel time-tagged counting.

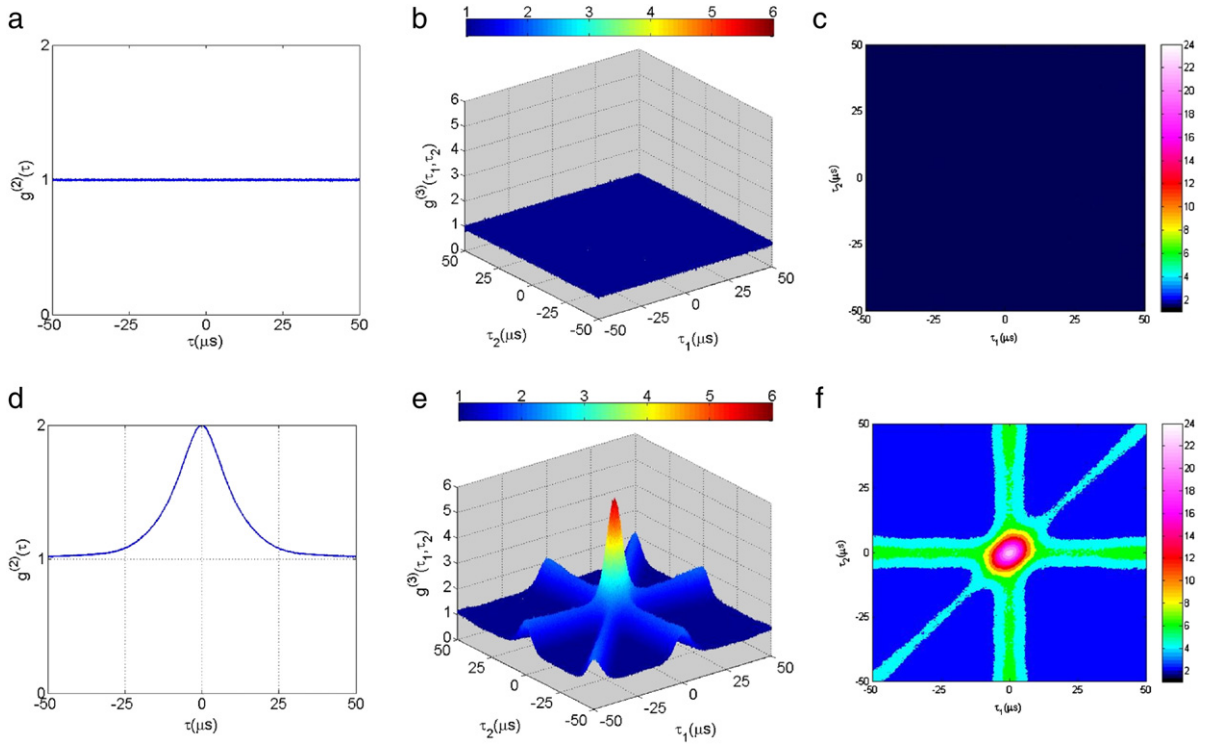

Fig. 24. The measured results. (a), (b) and (c) are $g^2(\tau)$, $g^3(\tau_1, \tau_2)$, $g^4(\tau_1, \tau_2, \tau_3)$ at $\tau_3 = 0$ μs for the coherent photon source, respectively; (d), (e) and (f) are $g^2(\tau)$, $g^3(\tau_1, \tau_2)$, $g^4(\tau_1, \tau_2, \tau_3)$ at $\tau_3 = 0$ μs for the pseudo-thermal photon source, respectively.

One important issue in this measurement is the influence of noise counts in the single photon detectors. As discussed earlier, in an up-conversion single photon detector, most noise photons are from the frequency conversion process, which is widely believed to be the Raman scattering in the PPLN waveguide caused by the strong pump beam. The intrinsic dark count rate of the Si-APD is very small and is negligible in our experiments. To determine the statistical nature of the noise

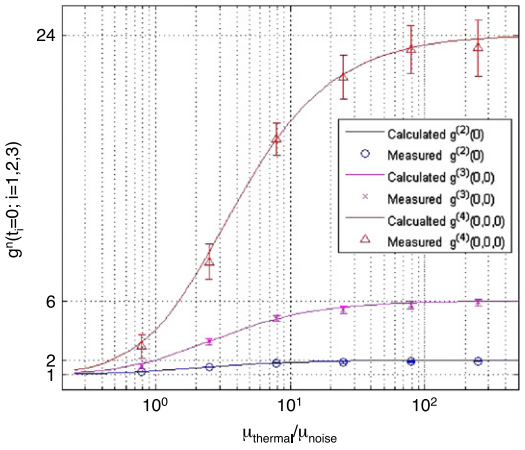

Fig. 25. The measured and calculated values of $g^{(2)}(0)$, $g^{(3)}(0, 0)$ and $g^{(4)}(0, 0, 0)$ for a thermal source as the SNR varies. The measured values are shown with the standard deviation error bars. $\mu_{thermal}$ and μ_{noise} are the mean photon number of a thermal source and noise respectively.

photons, we measured 2nd, 3rd and 4th order temporal correlations for the dark counts when the light source at 1310 nm is turned off and observed $g^{(n)} \approx 1$ ($n = 2, 3,$ and 4), demonstrating that there is no photon bunching at the origin of the noise photons. The results suggest that the statistics of the noise photons, at least approximately, follow a Poisson distribution for the time scale used in the experiments. Based on these results, it is possible to study the influence of noise counts in photon correlation measurements by varying the ratio of the signal count rate to dark count rate. For signal counts of pseudo-thermal photons obeying the Bose–Einstein distribution mixed with noise counts obeying Poisson distribution, the probability density function for n photons is the summation of the probability of signal counts and the probability of noise counts when the number of total photons from both sources is n. Accordingly, the temporal correlations for mixed signal and noise counts can be theoretically calculated. On the other hand, we are able to measure the values of $g^{(2)}(0)$, $g^{(3)}(0, 0)$ and $g^{(4)}(0, 0, 0)$ at different SNR levels for a thermal photon source. Fig. 25 shows the measured results and calculated values, which are in good agreement. By using background subtraction, a more accurate temporal correlation of signal photons can be obtained.

3.6. Optical sampling for single photons in frequency up-conversion

When the frequency up-conversion detector is operated in a pulsed pump mode, the pump pulse width is usually larger than the signal pulse width so that the pump pulse can completely cover the signal pulse and ensure an efficient frequency conversion. In this section we will discuss another case, in which a pump pulse width is narrower than the signal pulse width, thus acting as an optical gate. The pump pulse determines the gate width. When the gate width is much narrower than the signal width the process becomes an optical sampling scheme and is useful for time resolved measurements. As we mentioned in Section 3.2, a picosecond optical-sampling technique has been demonstrated for a strong light signal in a number of studies [41,42] and femtosecond optical sampling has been demonstrated in an up-conversion system using pump pulses as short as 150 fs [43].

By using the up-conversion technique, we demonstrated an optical sampling process at the single photon level. In this process the signal photon wavelength is converted and the amplitude profile of the photon wave packet is simultaneously modulated by the pump pulse shape. This is a direct consequence of the SHG in nonlinear optical materials. In our experiment, a set up similar to that described in Section 3.4 was used. A quantum dot was excited by a pulsed laser at 780 nm and emitted single photons at 1310 nm. The single photons at 1310 nm are then converted to 710 nm in a PPLN waveguide by using a pump wavelength at 1550 nm. Fig. 26 shows the photoluminescence histograms of the 710-nm up-converted photons. The curve in blue represents the histogram of up-converted photons using a CW pump and the curve in maroon records the histogram of up-converted photons when a 260-ps pulsed pump (see inset) at 1550 nm is used.

In our experiment, the delay between the arrival of the QD single photon and pump pulse can be varied. Fig. 27 shows the result of such a measurement for various delays from 0.0 to 3.5 ns using a 260-ps pulsed pump. The peaks nicely correspond to the decay curve of the CW profile, shown in blue for comparison. This measurement suggests that pulsed frequency up-conversion may be used for achieving high timing resolution in experiments on single quantum emitters. As we mentioned in Section 3.2, temporal resolution of the up-conversion technique is mostly limited by the jitter of the Si-APD, which is typically $>$ 50 ps. On the other hand, the time-domain sampling enabled by pulsed up-conversion provides a time resolution set by the pulse width, which is limited by the acceptance bandwidth for the QPM in the waveguide. For the 5-cm long PPLN waveguide used in our experiment, the acceptance bandwidth is 0.35 nm corresponding to a minimum pulse width of 10 ps in the time domain. Sub-picosecond time resolution can be achieved in broader bandwidth up-conversion systems [59], though a broader bandwidth device uses a shorter nonlinear chip and therefore may incur lower up-conversion efficiency.

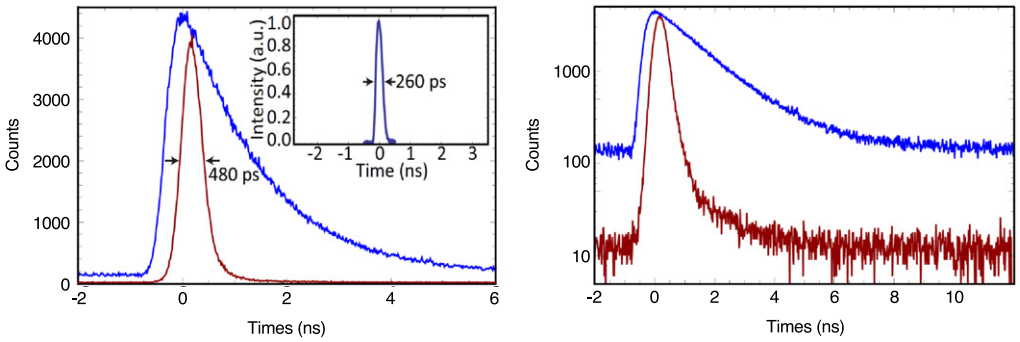

Fig. 26. Temporal profile of the up-converted photons pumped by a CW (blue) and 260-ps pulsed (maroon) light source at 1550 nm. The recorded photon counts are shown on linear (left) and log (right) scales. All measurements are taken with 1200 s integration. The inset is a 260-ps pump pulse measured by an optical communication analyzer. (For interpretation of the references to colour in this figure legend, the reader is referred to the web version of this article.)

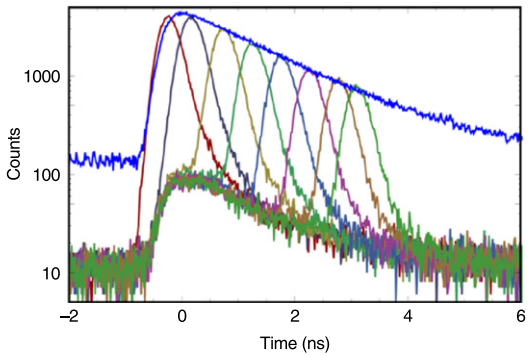

Fig. 27. Temporal profile of the up-converted photons at 710 nm. The peaks of the curves in various colors were recorded using a 260-ps pulsed pump at time delays of 0.0, 0.5, 1.0, 1.5, 2.0, 2.5 3.0 and 3.5 ns. All measurements are taken with 1200 s integration. The curve in blue is recorded using a CW pump at 1550 nm. (For interpretation of the references to colour in this figure legend, the reader is referred to the web version of this article.)

The integration of disparate quantum systems is an ongoing effort in the development of distributed quantum networks. Two challenges in such hybrid schemes are the differences in transition frequencies and linewidths among the component systems. For example, QD-generated single photons have a coherence time that is typically less than twice its lifetime, and they are not perfectly indistinguishable due to the interaction of the confined carriers in the QD with the surrounding crystal field. The short coherence time and imperfect indistinguishable single photon states prevents integration using single photons from nonidentical QDs. As a solution, simultaneous frequency conversion and amplitude modulation can be used to generate indistinguishable single photons from nonidentical QDs. Frequency conversion can translate the wavelengths of each of the single photons to the same wavelength with a spectral bandwidth "engineered" in a process of spectral filtering by the QPM acceptance bandwidth. Together with amplitude modulation it is possible to create indistinguishable single photons from QDs spectrally separated by the entire inhomogeneous linewidth of the QD distribution without the need for electrical gates or modification of the sample. In essence, frequency up-conversion plays the role of a passive interface between two interacting photons from independent sources and makes possible the integration of disparate quantum systems. Furthermore, the frequency up-conversion technique enables, in principle, an interaction between single photons at telecommunication wavelengths (as flying qubits) and atomic transitions suitable for use in quantum memory (as stationary qubits) that are usually in the visible or near visible regions.

4. Prospects and discussions

As the results described in this paper have demonstrated, single photon frequency up-conversion technology has been successfully applied to a variety of quantum information systems and applications. Moreover, this technology can be further applied to many important areas relating to quantum computation and communication. In this section we will describe some of these areas.

Significant attention has been given to the integration of disparate quantum systems towards future quantum networks [64] or quantum repeaters. These systems consist of quantum processors and quantum memories. Photons have proved to

be suitable for transmitting quantum information (flying qubits) while atoms and ions have the ability to store and process quantum information (stationary qubits). Connecting these flying qubits and stationary qubits at different wavelengths becomes an important challenge for the development of such systems. Photonic quantum information interfaces [65,66] based on SPDC were proposed and recently demonstrated. These SPDC based types of quantum interfaces can be considered to be active quantum interfaces because the signal photons are generated by the interface at the wavelength of interest. In an active quantum interface, a pump beam generates non-degenerate photon pairs by SPDC in a nonlinear material. One photon in the pair is at telecommunications wavelength; the other is tuned to the atomic absorption line and therefore must be spectrally very narrow — in the order of megahertz. However, due to the nature of the SPDC process, the output linewidth, typically several hundreds of gigahertz, is a few orders of magnitude broader than the absorption linewidth of the atomic transitions required for quantum processing or quantum memories.

Based on the up-conversion devices, it is possible to develop another type of interface which can be considered to be passive interfaces. A passive quantum interface does not generate signal photons at the wavelength of interest; instead, it converts signal wavelengths to the required wavelength. In most cases, an up-conversion unit converts signal photons in the telecommunication wavelengths to a new wavelength which corresponds to the central wavelength and linewidth of an atomic transition line used in a quantum signal processor or quantum memory. Such an approach was proposed in 2002 for a long distance single photon teleportation [67]. In general, by using a tunable pump source with a very narrow linewidth, any signal photons can always be precisely converted to a suitable wavelength with high conversion efficiency and low noise. More importantly, the converted photons preserve the quantum features of the original photons. As a result, the passive quantum interface makes it possible for the interaction between flying qubits and stationary qubits.

In quantum communication or quantum computation research, the quantum systems are connected by measuring the interference of photon pairs from the two systems. A successful measurement of two-photon interference requires the two photons be non-distinguishable, meaning that they have identical wavelength, phase (coherence time), and polarization and that they arrive at same time. These are very severe restrictions. For example, the wavelengths of two photons from two QDs are not always at the exact same wavelength. In order to observe such photon interference, one NIST research group applied pressure to one QD to tune its wavelength in order to match the other QD [68]. Another similar interference experiment was performed on photons from a QD and a SPDC process in a nonlinear crystal [69]. A volume Bragg grating was used to change the spectral linewidth (therefore coherence time) of the SPDC generated photons to match the linewidth of the photons generated by the QD. A passive quantum interface can play the same role. When two up-conversion units are equipped with tunable pumps and used to convert photon pairs from two independent sources, their different wavelengths (separated by as much as tens of nm) can be precisely converted to a suitable third wavelength. Additionally, the coherence time of such photons can be modified by a pulsed pumping scheme in up-conversion units as described in Section 3.6. As a result, a better interference visibility can be obtained. Passive quantum interfaces therefore have great potential for modifying photonic qubits from independent sources for better photon interference measurements.

There is yet another unique feature of up-conversion devices — the ability to be used as a quantum optical switch. In, Section 3.2, we demonstrated up-conversion using a multi-wavelength pumping scheme. This approach divides the minimum resolvable time period into sub-periods, and then projects them into the wavelength domain, which can then be separated using dispersive elements. The separated photons at different wavelengths can be directed to propagate in different directions and the device can be considered an optical switch. The process of switching between pump wavelengths is an electronic process and typically very fast. Based on this feature, we can develop a $1 \times N$ fast optical switch with simultaneous wavelength conversion. This can be a useful tool in many areas of quantum information research. For example, this fast optical switch can be used to actively and randomly select the measurement bases for a QKD system.

While up-conversion devices have many good features and offers potential in many applications, some limitations and challenges exist that need to be considered. Firstly, the overall detection efficiency of the up-conversion detector is dependent on the detection efficiency of the final detection device, such as a Si-APD, and is further limited by the total system losses including losses in the PPLN waveguide and in the optical path. The peak detection efficiency for a commercially available Si-APD is in the range of 65 % to 70%. The total system loss is in the range of 3 dB. Though the internal conversion efficiency inside the waveguide can reach almost 100%, the overall detection efficiency of an up-conversion detector is significantly less than that in practical cases, considering the 3 dB losses and typical detection efficiency of the Si-APD, a total up-conversion detector efficiency of over 30% can be achieved. Secondly, dark counts, which are mainly created by Raman scattering in the waveguide by the strong pump, limits the effective sensitivity of the system. Although we have demonstrated a low dark count rate of 650 counts/s at the peak conversion efficiency, any further reduction of its dark count rate is a significant challenge. Thirdly, up-conversion detectors are polarization sensitive and can only detect photons with a certain polarization orientation. This problem can be solved using two perpendicularly arranged PPLN waveguides [70], resulting in a more costly and complicated system. Finally, in the application of an up-conversion spectrometer, the resolution is limited by the acceptance linewidth of the PPLN waveguide. As a result, especially when measuring narrow linewidth spectra, the high orders of the transfer function of QPM appear as fake side-peaks in the measured spectrum. These however may be removed using complicated de-convolution algorithms.

Single photon frequency up-conversion has many potential advantages for use in quantum communication systems, and we expect that this technology will become an important tool in quantum communication and quantum networking in the future.

5. Conclusion

Based on frequency sum generation in nonlinear optical materials, we have developed single photon up-conversion detectors for telecommunication wavelengths. By tuning the pump wavelength, an ultra sensitive single photon spectrometer was implemented for wavelengths near 1310 nm. We successfully used the up-conversion detectors and the spectrometer in a wide variety of research projects. A QKD system at 1310 nm equipped with up-conversion detectors was capable of generating secure keys in real time for one-time-pad encryption of continuous 200-kbit/s encrypted streaming video signals transmitted over 10 km. To further increase the QKD key rate, it is necessary to improve the system temporal resolution that is originally limited by the jitter of the Si-APD. We proposed and experimentally demonstrated an optical sampling approach using multiple spectrally and temporally distinct pump pulses to enable a higher system temporal resolution beyond the jitter limitation of the Si-APD used in the system. The up-conversion detectors and spectrometer were used to characterize photon sources including a time-bin entangled photon pair source from SPDC and single photons from a semiconductor quantum dot. We tested the time-bin entanglement and measured the emission spectra of the single photons near 1310 nm for both systems. The QD lifetime measurement using our up-conversion detector shows a dynamic range of about 25 times better than that using a commercial InGaAs APD and therefore achieves a higher accuracy measurement. The second order temporal correlation measurement for single photons from a QD proves that the quantum nature of the single photons is preserved in the frequency up-conversion process. We further demonstrated the preservation of the quantum state during up-conversion by our measurements of high-order (2nd, 3rd and 4th) temporal correlation of single photons from coherent and pseudo-thermal sources. By using a short pulse pumping scheme in an up-conversion detector, a time-resolved measurement for the temporal amplitude profile of single photons from a QD was performed. The results of this work also shows the possibility that simultaneous frequency translation followed by spectral filtering and amplitude modulation can be used to generate indistinguishable single photons from non-identical QDs. In principle, frequency up-conversion can play a role of a passive interface connecting two single photons from independent sources and makes possible the integration of disparate quantum systems.

In conclusion, the frequency up-conversion technique is a useful and practical approach for low noise and high efficiency single photon detection in the NIR region and it can be widely used in many advanced research areas as well as for practical applications.

Acknowledgments

This work was supported by the NIST quantum information initiative. We wish to thank Hai Xu, Alan Mink, Barry Hershman, Tassos Nakassis of ITL, NIST, and Joshua Bienfang from PML, NIST, for important contributions to QKD system with up-conversion detectors. We also thank Qiang Zhang, Jason Pelc, Carsten Langrock and Martin Fejer of Stanford University, for collaboration and technical discussion on up-conversion spectrometer. The research on up-conversion of photons from quantum dots was a collaboration with Matthew Rackher and Kartik Srinivasan of CNST, NIST; the research on multi-wavelength pump sampling technology was a collaboration with Joshua Bienfang of PML, NIST; the research on high order correlation following up-conversion was a collaboration with Matthew Rackher and Kartik Srinivasan of CNST, NIST and Martin Stevens of PML, NIST. Burm Baek of PML, NIST, provided high order correlation calculation programs.

References

[1] M.D. Eisamanw, J. Fan, A. Migdall, S.V. Polyakov, Rev. Sci. Instrum. 82 (2011) 071101.
[2] R.H. Hadfield, Nat. Photonics 3 (2009) 696.
[3] Z.L. Yuan, A.R. Dixon, J.F. Dynes, A.W. Sharpe, A.J. Shields, Appl. Phys. Lett. 92 (2008) 201104.
[4] A.E. Lita, A.J. Miller, S.W. Nam, Opt. Express 16 (2008) 3032.
[5] H. Takesue, S.W. Nam, Q Zhang, R.H. Hadfield, T. Honjo, K. Tamaki, Y. Yamamoto, Nat. Photonics 1 (2007) 343.
[6] Q. Zhang, H. Takesue, S.W. Nam, C. Langrock, B. Baek, M. Fejer, Y. Yamamoto, Opt. Express 16 (2008) 5776.
[7] L. Ma, S.W. Nam, H. Xu, B. Baek, T. Chang, O. Slattery, A. Mink, X. Tang, New J. Phys. 11 (2009) 054020.
[8] K.M. Rosfjord, J.K.W. Yang, E.A. Dauler, A.J. Kerman, V. Anant, B.M. Voronov, G.N. Gol'tsman, K.K. Berggren, Opt. Express 14 (2006) 527.
[9] J. Midwinter, J. Warner, J. Appl. Phys. 38 (1967) 519.
[10] P. Kumar, Opt. Lett. 15 (1990) 1476.
[11] J. Huang, P. Kumar, Phys. Rev. Lett. 68 (1992) 2153.
[12] Y. Kim, S.P. Kulik, Y. Shih, Phys. Rev. Lett. 86 (2001) 1370.
[13] A.P. Vandevender, P.G. Kwiat, J. Modern Opt. 51 (2004) 1433.
[14] M. Albota, F. Wong, Opt. Lett. 29 (2004) 1449.
[15] C. Langrock, E. Diamanti, R.V. Roussev, Y. Yamamoto, M. Fejer, H. Takesue, Opt. Lett. 30 (2005) 1725.
[16] E. Diamanti, H. Takesue, T. Honjo, K. Inoue, Y. Yamamoto, Phys. Rev. A 72 (2005) 052311.
[17] R.T. Thew, S. Tanzilli, L. Krainer, S.C. Zeller, A. Rochas, I. Rech, S. Cova, H. Zbinden, N. Gisin, New J. Phys. 8 (2006) 32.
[18] H. Xu, L. Ma, X. Tang, Optics East 07, Proc. SPIE. 6780 (2007) 67800U-1.
[19] L. Ma, O. Slattery, X. Tang, Opt. Express 17 (2009) 14395.
[20] H. Xu, L. Ma, A. Mink, B. Hershman, X. Tang, Opt. Express 15 (2007) 7247.
[21] L. Ma, J. Bienfang, O. Slattery, X. Tang, Optics Express 19 (2011) 5470.
[22] L. Ma, O. Slattery, T. Chang, X. Tang, Optics Express 17 (2009) 15799.
[23] M.T. Rakher, L. Ma, O. Slattery, X. Tang, K. Srinivasan, Nat. Photonics 4 (2010) 786.
[24] L. Ma, M.T. Rakher, M. Stevens, O. Slattery, K. Srinivasan, X. Tang, Opt. Express 19 (2011) 10501.
[25] M.T. Rakher, L. Ma, M. Davanco, O. Slattery, X. Tang, K. Srinivasan, Phys. Rev. Lett. 107 (2011) 083602.
[26] Y.R. Shen, The Principle of Nonlinear Optics, Wiley-Interscience, ISBN: 0 471-88998-9, 1984.

[27] Amnon Yariv, Pochi Yeh, Optical Waves in Crystals, Wiley-Interscience, ISBN: 0 471-09142-1, 1983.
[28] L.E. Myers, R.C. Eckardt, M.M. Fejer, R.L. Byer, J. Opt. Soc. Am. B 12 (1995) 2102.
[29] K.R. Parameswaran, J.R. Kurz, R.V. Roussev, M.M. Fejer, Opt. Lett. 27 (2002) 43.
[30] M. Fejer, G. Magel, D. Jundt, R. Byer, IEEE J. Quantum Electron. 28 (1992) 2631.
[31] R.V. Roussev, C. Langrock, J.R. Kurz, M.M. Fejer, Opt. Lett. 29 (2004) 1518.
[32] Datasheet of Perkin Elmer Single Photon Counting Module SPCM-AQR Series.
[33] J.S. Pelc, C. Langrock, Q. Zhang, M. Fejer, Opt. Lett. 35 (2010) 2804.
[34] J.S. Pelc, L. Ma, C.R. Phillips, Q. Zhang, C. Langrock, O. Slattery, X. Tang, M. Fejer, Opt. Express 19 (2011) 21445.
[35] Q. Zhang, C. Langrock, M. Fejer, Y. Yamamoto, Opt. Express 16 (2008) 19557.
[36] N. Gisin, G. Ribordy, W. Tittel, H. Zbinden, Rev. Modern Phys. 74 (2002) 145.
[37] C.H. Bennett, Phys. Rev. Lett. 68 (1992) 3121.
[38] A. Mink, L. Ma, T. Nakassis, H. Xu, O. Slattery, B. Hershman, X. Tang, ICQNM 2008 (2008) 16.
[39] A. Mink, X. Tang, L. Ma, T. Nakassis, B. Hershman, J. Bienfang, D. Su, R. Boisvert, C.W. Clark, C.J. Williams, Proc. SPIE 6244 (2006) 62440M-1.
[40] A. Mink, J. Bienfang, R. Carpenter, L. Ma, B. Hershman, A. Restelli, X. Tang, New J. Phys. 11 (2009) 054016.
[41] H. Ishizuki, T. Suhara, M. Fujimura, H. Nishihara, Opt. Quantum Electron. 33 (2001) 953.
[42] P.A. Andrekson, M. Westlund, Laser & Photonics Rev. 1 (2007) 231.
[43] O. Kuzucu, F.N. Wong, S. Kurimura, S. Tovstonog, Opt. Lett. 33 (2008) 2257.
[44] J. Huang, C. Langrock, X. Xie, M. Fejer, Opt. Lett. 32 (2007) 2420.
[45] A. Restelli, J.C. Bienfang, A. Mink, C. Clark, Proc. SPIE 7236 (2009) 72360L.
[46] L. Ma, S. Nam, H. Xu, B. Baek, T. Chang, O. Slattery, A. Mink, X. Tang, New J. Phys. 11 (2009) 045020.
[47] Masaki Asobe, Osamu Tadanaga, Hiroshi Miyazawa, Yoshiki Nishida, Hiroyuki Suzuki, Opt. Lett. 28 (2003) 558.
[48] J. Brendel, N. Gisin, W. Tittel, H. Zbinden, Phys. Rev. Lett. 82 (1999) 2594.
[49] I. Marcikic, H. Ridmatten, W. Tittel, H. Zbinden, N. Gisin, Phys. Rev. Lett. 93 (2004) 180502.
[50] H. Takesue, K. Inoue, Phys. Rev. A 72 (2005) 041804.
[51] T. Honjo, H. Takesue, H. Kamad, Y. Nishida, O. Tadanaga, M. Asobe, K. Inoue, Opt. Express 15 (2007) 13957.
[52] Q. Zhang, C. Langrock, H. Takesue, X. Xie, M. Fejer, Y. Yamamoto, Opt. Express 16 (2008) 3293.
[53] J. Franson, Phys. Rev. Lett. 62 (1989) 2205.
[54] I. Marcikic, H. Riedmattern, W. Tittel, V. Scarani, H. Zbinden, N. Gisin, Phys. Rev. A 66 (2002) 062308.
[55] J. Clauser, M. Horne, A. Shimony, R. Holt, Phys. Rev. Lett. 23 (1969) 880.
[56] A.P. Van Devender, P.G. Kwiat, J. Opt. Soc. Am. B 24 (2007) 295.
[57] S. Tanzilli, W. Tittel, M. Halder, O. Alibart, P. Baldi, N. Gisin, H. Zbinden, Nature 437 (2005) 116.
[58] K. Srinivasan, O. Painter, A. Stintz, S. Krishna, Appl. Phys. Lett. 91 (2007) 091102.
[59] C. Santori, D. Fattal, J. Vuckovic, G.S. Solomon, E. Waks, Y. Yamamoto, Phys. Rev. B 69 (2004) 205324.
[60] R. Hanbury-Brown, R.Q. Twiss, Nature 177 (1956) 27.
[61] M. Fox, Quantum Optics, An introduction, Oxford university press, 2006.
[62] Y. Zhou, J. Liu, Y. Shih, arXiv: 0909.3512v1 [quant-ph] 2009.
[63] M.J. Stevens, B. Baek, E. Dauler, A. Kerman, R. Molnar, S.A. Hamilton, K.K. Berggren, R.P. Mirin, S.W. Nam, Opt. Express 18 (2) (2010) 1430.
[64] H.J. Kimble, Nature 453 (2008) 1023.
[65] S. Tanzilli, W. Tittel, M. Halder, O. Alibart, P. Baldi, N. Gisin, H. Zbinden, Nature 437 (2005) 116.
[66] R. Ikuta, Y. Kusaka, T. Kitano, H. Kato, T. Yamamoto, M. Koashi, N. Imoto, Nature Communications 2 (2011) 537.
[67] Jeffrey H. Shapiro, New J. Phys. 4 (2002) 47.
[68] E.B. Flagg, A. Muller, S. Polyakov, A. Ling, A. Migdall, G.S. Solomon, Phy. Rev. Lett. 104 (2010) 137401.
[69] S. Polyakov, A. Muller, E.B. Flagg, A. Ling, N. Borjemscaia, E.V. Keuren, A. Migdall, G.S. Solomon, Phy. Rev. Lett. 107 (2011) 157402.
[70] L. Ma, O. Slattery, X. Tang, Laser Physics 20 (2010) 1612.